Quaternary Science Reviews 29 (2010) 113–128

Contents lists available at ScienceDirect

Quaternary Science Reviews

journal homepage: www.elsevier.com/locate/quascirev

EPICA Dome C record of glacial and interglacial intensities

V. Masson-Delmotte [a,*], B. Stenni [b], K. Pol [a], P. Braconnot [a], O. Cattani [a], S. Falourd [a], M. Kageyama [a], J. Jouzel [a], A. Landais [a], B. Minster [a], J.M. Barnola [c], J. Chappellaz [c], G. Krinner [c], S. Johnsen [d], R. Röthlisberger [e], J. Hansen [f,g], U. Mikolajewicz [h], B. Otto-Bliesner [i]

[a] Laboratoire des Sciences du Climat et de l'Environnement, IPSL, UMR CEA CNRS UVSQ 1572, CEA Saclay, Bât. 701, L'Orme des Merisiers, 91 191 Gif-sur-Yvette cédex, France
[b] Università di Trieste, Dipartimento di Scienze Geologiche, Ambientali e Marine, Via E. Weiss 2, 34127 Trieste, Italy
[c] Laboratoire de Glaciologie et Géophysique de l'Environnement, UMR CNRS UJF 5183, 54 rue Molière, 38 402 Saint Martin d'Hères cédex, France
[d] Geophysical Department, Juliane Maries Vej 30, DK-2100 Kobenhavn, Denmark
[e] British Antarctic Survey, High Cross, Madingley Road, Cambridge CB3 0ET, United Kingdom
[f] NASA/Goddard Institute for Space Studies, New York, NY 10025, USA
[g] Columbia University Earth Institute, New York, NY 10027, USA
[h] Max-Planck-Institute for Meteorology, Bundesstrasse 53, D-20146 Hamburg, Germany
[i] CCR, CGD/NCAR, PO Box 3000, Boulder, CO 80307-3000, USA

ARTICLE INFO

Article history:
Received 19 December 2008
Received in revised form
29 September 2009
Accepted 30 September 2009

ABSTRACT

Climate models show strong links between Antarctic and global temperature both in future and in glacial climate simulations. Past Antarctic temperatures can be estimated from measurements of water stable isotopes along the EPICA Dome C ice core over the past 800 000 years. Here we focus on the reliability of the relative intensities of glacial and interglacial periods derived from the stable isotope profile. The consistency between stable isotope-derived temperature and other environmental and climatic proxies measured along the EDC ice core is analysed at the orbital scale and compared with estimates of global ice volume. MIS 2, 12 and 16 appear as the strongest glacial maxima, while MIS 5.5 and 11 appear as the warmest interglacial maxima.

The links between EDC temperature, global temperature, local and global radiative forcings are analysed. We show: (i) a strong but changing link between EDC temperature and greenhouse gas global radiative forcing in the first and second part of the record; (ii) a large residual signature of obliquity in EDC temperature with a 5 ky lag; (iii) the exceptional character of temperature variations within interglacial periods.

Focusing on MIS 5.5, the warmest interglacial of EDC record, we show that orbitally forced coupled climate models only simulate a precession-induced shift of the Antarctic seasonal cycle of temperature. While they do capture annually persistent Greenland warmth, models fail to capture the warming indicated by Antarctic ice core δD. We suggest that the model-data mismatch may result from the lack of feedbacks between ice sheets and climate including both local Antarctic effects due to changes in ice sheet topography and global effects due to meltwater–thermohaline circulation interplays. An MIS 5.5 sensitivity study conducted with interactive Greenland melt indeed induces a slight Antarctic warming. We suggest that interglacial EDC optima are caused by transient heat transport redistribution comparable with glacial north–south seesaw abrupt climatic changes.

1. Introduction

Glacial–interglacial climate change is expected to result from the orbital forcing, changes in atmospheric composition and internal feedbacks, such as changes in planetary albedo (Paillard, 1998). Along the last million years, changes in land–sea geographical distribution can be considered as negligible in driving past changes in climate and atmospheric composition, in contrast with deeper times. Over this time period, the orbital forcing is well known from astronomical calculations (Berger and Loutre, 1991; Laskar et al., 1993). It is therefore critical to document the relative intensities of past glacial and interglacial periods, in terms of changes in atmospheric composition and global temperatures. Each climate archive provides a complementary view of the global

* Corresponding author. Tel.: +33 1 69 08 77 15; fax: +33 1 69 08 77 16.
E-mail address: valerie.masson@cea.fr (V. Masson-Delmotte).

0277-3791/$ – see front matter © 2009 Elsevier Ltd. All rights reserved.
doi:10.1016/j.quascirev.2009.09.030

climate system. Globally relevant climate data can be extracted from marine records, where proxies document past changes in tropical sea surface temperature (Lea, 2004), deep ocean temperature (Zachos et al., 2001), or past changes in sea level (Bintanja et al., 2005; Lisiecki and Raymo, 2005), or from continental records documenting past changes in vegetation cover (Cheddadi et al., 2005; Tzedakis et al., 2006) or monsoon intensity (Sun et al., 2006; Wang et al., 2008).

There are specific areas, such as the tropics or Antarctica (Fig. 1), where climate models show a strong link between local temperature changes and global temperature changes (Lea, 2004; Masson-Delmotte et al., 2006a; Schneider von Deimling et al., 2006; Hargreaves et al., 2007; IPCC, 2007). Here, we focus on deep Antarctic ice cores. They offer a variety of new climate and environmental records including the documentation of past atmospheric composition over several glacial–interglacial cycles, at Vostok (Petit et al., 1999), Dome Fuji (Watanabe et al., 2003; Kawamura et al., 2007) or EPICA Dome C (Jouzel et al., 2007; Loulergue et al., 2008; Lüthi et al., 2008). Recently, multiple parameters have been measured on the EPICA Dome C (hereafter EDC) ice core spanning the past 800 000 years (Section 2).

These parameters track climate changes from a variety of latitudes. Past temperatures are relevant for central Antarctica. Past changes in sea salt sodium have been suggested to be related to sea ice surface area, modulated by uplift and transport from the sea ice surface towards central Antarctica. Past changes in methane concentrations are relevant for continental wetland temperature and moisture, mainly in the tropics and the Northern Hemisphere. Past changes in carbon dioxide concentration are relevant for changes in terrestrial and marine carbon sources and sinks, and past changes in dust or non-sea-salt calcium are expected to document dust production on southern hemisphere mid-latitude continents and its transport to Antarctica. Recent studies have been conducted on the sequence of events during terminations (Röthlisberger et al., 2008), but this approach remains difficult to extend to the phase relationships between atmospheric composition and climate due to relative dating uncertainties for the gas and the ice records caused by firnification processes (Caillon et al., 2003; Loulergue et al., 2007).

Section 3 is focused on the relative intensity of glacial and interglacial extrema as identified in various ice core proxies. First, we discuss the uncertainties on past Antarctic temperatures which are estimated from measurements of water stable isotopes along the EPICA EDC ice core over the past 800 000 years. We then discuss the consistency between stable isotope-derived temperature and other environmental and climatic proxies measured in the EDC ice core regarding the relative intensity of glacial and interglacial extrema.

Section 4 is dedicated to the links between radiative perturbations and climate and the new results from the EDC ice core. We discuss the weights of orbital frequencies in EDC temperature. We analyse the links between EDC temperature and greenhouse gas radiative forcing. We use climate models to discuss the relationship between Antarctic and global temperature, highlighting the problems of changes in local ice sheet elevation. A reconstruction of past global temperature variations is compared to the simulations of global temperature response to global radiative forcings estimated from past changes in greenhouse gas concentrations and in northern hemisphere glaciation.

As we show that EDC interglacial temperature variations cannot be explained by a simple response to radiative forcing perturbations, we finally focus our discussion (Section 5) on the warmest interglacial period identified in the EDC ice cores (MIS 5.5). We compare the response of climate models forced by changes in orbital configurations with observational constraints from Greenland and Antarctica. We show that MIS 5.5 Antarctic warmth is not captured by the response of ocean and atmosphere dynamics to orbital forcing and that other feedbacks involving the coupling with the cryosphere must be at play.

2. Data

In this analysis, we use the available datasets measured and previously published, on the EPICA EDC3 age scale (Parrenin et al., 2007a). This age scale is generated by combining an accumulation and an ice flow model optimised using absolute age markers (Parrenin et al., 2007b). For the time period from 300 to 800 kyr (thousands of years before present), the age scale is obtained from a glaciological interpolation of precession age markers identified in EDC $\delta^{18}O$ of O_2 (Dreyfus et al., 2007). The accuracy of the EDC3 age scale is estimated to be ~6 kyr from 130 kyr to 800 kyr. The EDC3 age scale is therefore set up independently of the orbital properties of δD.

The δD measurements of the ice core are available on 55 cm ice sections ("bag samples") (Jouzel et al., 2007). Due to the combined

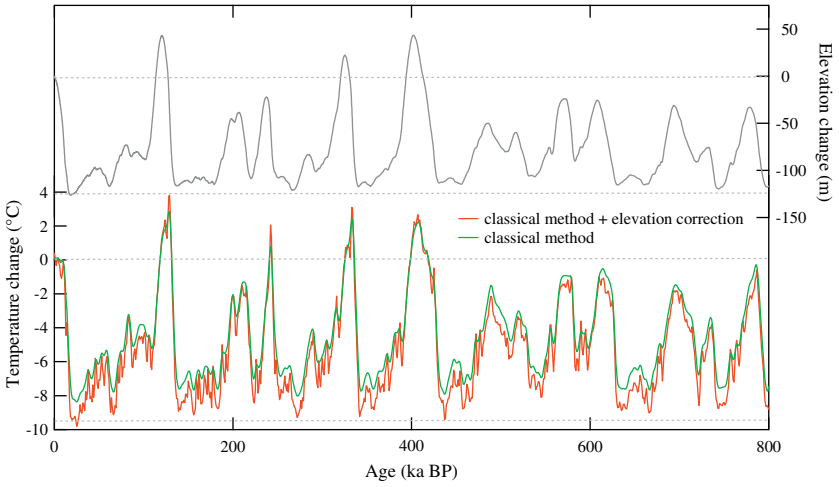

Fig. 1. Comparison of two methods to assess past EDC temperature based on EDC ice core δD. Green, conventional approach taking into account past changes in sea water isotopic composition and a constant isotope–temperature slope. Red (Jouzel et al., 2007), same as green but also including a correction for ice sheet elevation changes derived from the glaciological model used for the age scale, displayed in grey on the top panel (Parrenin et al., 2007b). Horizontal dashed lines show the average Holocene and Last Glacial Maximum levels.

effects of lower glacial accumulation and ice thinning, this depth resolution corresponds to a temporal resolution of ~20 years during the Holocene, ~50 years during MIS 2, ~200 years during MIS 11, ~600 years during MIS 12 and ~1000 years during the oldest glacial periods. As the average temporal spacing is ~150 years, we have re-sampled the data to a mean 200 year resolution.

The CO_2 record discussed here is constructed with a stack of concentration measurements combined from the Vostok (Petit et al., 1999) and EPICA DC ice cores (Monnin et al., 2001; Siegenthaler et al., 2005; Lüthi et al., 2008), transferred onto the EDC3 age scale. The methane profile is now continuously available from the EDC ice core (Spahni et al., 2005; Loulergue et al., 2008). Hereafter, we use them either in terms of concentrations, or in terms of radiative forcing, using a consensus conversion from concentration to radiative forcing (Joos, 2005). In the following equations, atmospheric concentrations are expressed in ppmv for CO_2 (respectively ppbv for CH_4) and the pre-industrial reference concentration $CO_{2,0}$ is 278 ppmv (respectively 742 ppbv for $CH_{4,0}$); radiative forcings are expressed in $W\,m^{-2}$; we neglect the correction term accounting for the overlap between CH_4 and N_2O absorption bands. The global Radiative Forcing (RF) caused by the different gases is then estimated by:

$$RF_{CO_2} = 5.35 \times \ln\left(\frac{[CO_2]}{[CO_{2,0}]}\right) \quad (1)$$

$$RF_{CH_4} = 0.036 \times \left(\sqrt{[CH_4]} - \sqrt{[CH_{4,0}]}\right) \quad (2)$$

The temporal resolution of the records is variable. From the Vostok data, the mean temporal interval between subsequent data is 1187 ± 1080 years for CO_2 (the largest gap between measurements is 8600 years). For Dome C, from 400 to 800 ka BP, the mean temporal interval between CO_2 data is 684 ± 406 years (maximum spacing of 3525 years). For EDC CH_4 data, the mean temporal interval is 381 ± 333 years (maximum spacing of 3460 years). The best documented periods have temporal resolutions up to 200 years. In order to be consistent with the mean spacing of the deuterium record, we have also re-sampled the stacked radiative forcing record on a 200 year time step.

The dust flux is documented by 989 data points back to 740 ka BP, corresponding to a mean age distance of 750 ± 1450 years (EPICA-Community-Members, 2004; Lambert et al., 2008). As Antarctic ice core dust levels are log-normally distributed, we have considered the logarithm of the dust flux as the function which should be most clearly related to the climate signal from dust source areas (Petit and Delmonte, 2009).

By comparison, the temporal resolution of the chemical records (Wolff et al., 2006) is slightly higher than the dust profile resolution (a total of 1400 depths sampled). It was recently expanded to 800 ka at 100 year resolution (Röthlisberger et al., 2008). The chemical composition of the ice in terms of calcium, sodium and sulphate is published on a 2.2 m depth basis, corresponding to 1405 depths and a mean temporal resolution of 530 ± 660 years. For consistency with the deuterium record, these profiles have also been re-sampled to a 200 year time interval.

The accumulation rate is derived from the inverse glaciological dating method (Parrenin et al., 2007a), mainly as the result of an optimised relationship with the deuterium content of the ice, which is supposedly related to the condensation temperature and the moisture-holding capacity of the atmosphere. We have used accumulation data at a 200 year time step to derive the atmospheric flux of aerosols from the observed concentrations of non-sea-salt calcium, sea salt sodium and dust. Note that while the accuracy of the measurements of stable isotopes or greenhouse gases is stable over glacials or interglacials, the very low levels of dust and aerosol fluxes during interglacial periods make the discussion of their variability within or between interglacials more difficult due to the low signal to noise ratios (see the envelope of the profiles in Fig. 2).

In order to compare the EDC records with a northern hemisphere perspective, we have included in our comparison the northern hemisphere ice volume derived from the marine sediment signals after correction for deep water temperature effects (Bintanja et al., 2005) using benthic stacks (Lisiecki and Raymo, 2005).

Note that the time step of 200 years was selected based on the average resolution of deuterium data. We have repeated our analyses using a lower time resolution of 1000 years: our results regarding glacial and interglacial intensities are robust with respect to this sampling resolution.

3. Relative intensity of glacial and interglacial EDC temperature changes

3.1. EDC temperature reconstructions

Fig. 1 shows different temperature reconstructions based on EDC stable isotope data. The detailed basis of temperature reconstructions using ice core isotopic composition has been previously published (Jouzel et al., 2003; Masson-Delmotte et al., 2006b; Masson-Delmotte et al., 2008). Due to isotopic distillation processes, changes in central Antarctic snow δD are primarily driven by changes in condensation temperature. Past temperature reconstructions rely on the explicit assumptions of a constant relationship between mean condensation and surface temperatures (including a constant inversion strength). Available isotopic modelling studies show that in central Antarctica the glacial–interglacial relationship between surface temperature and snow isotopic composition is similar to the modern spatial gradient (Jouzel et al., 2007). The EDC δD data have to be corrected for sea water isotopic composition changes linked with ice volume formation (Bintanja et al., 2005). A first temperature can then be estimated using the modern spatial isotope–temperature slope (Masson-Delmotte et al., 2008) and is referred to as "classical method". Several factors can have an additional impact on the temperature and are not accounted for in this "classical" reconstruction:

1. In order to provide climate information which is independent of variations of local elevation, a "fixed elevation" temperature reconstruction was recently produced (Jouzel et al., 2007). Past elevation variations can be estimated from the accumulation and ice flow model used for EDC dating (Parrenin et al., 2007b). EDC elevation is reduced by up to 125 m during glacial periods in response to reduced glacial accumulation, and enhanced by up to 45 m during "warm" interglacials such as MIS 5.5 (Fig. 1). The shapes and magnitudes of these modelled elevation changes are comparable with other independent glaciological calculations (Pollard and DeConto, 2009). In order to correct for elevation effects, we assume a constant lapse rate of 9 °C per km based on modern spatial gradients. The hypothesis of a constant lapse rate is supported by sensitivity studies conducted with the LMDz model with different glacial ice sheet configurations (see Section 4.3). The glacial–interglacial EDC temperature variations (at constant present-day altitude) are enhanced by ~1 °C (~10%) when considering elevation changes (Fig. 1). Early interglacials (before 420 ka) appear cooler than the most recent interglacials (since 420 ka), and the elevation correction enhances this temperature contrast (by ~0.5 °C).

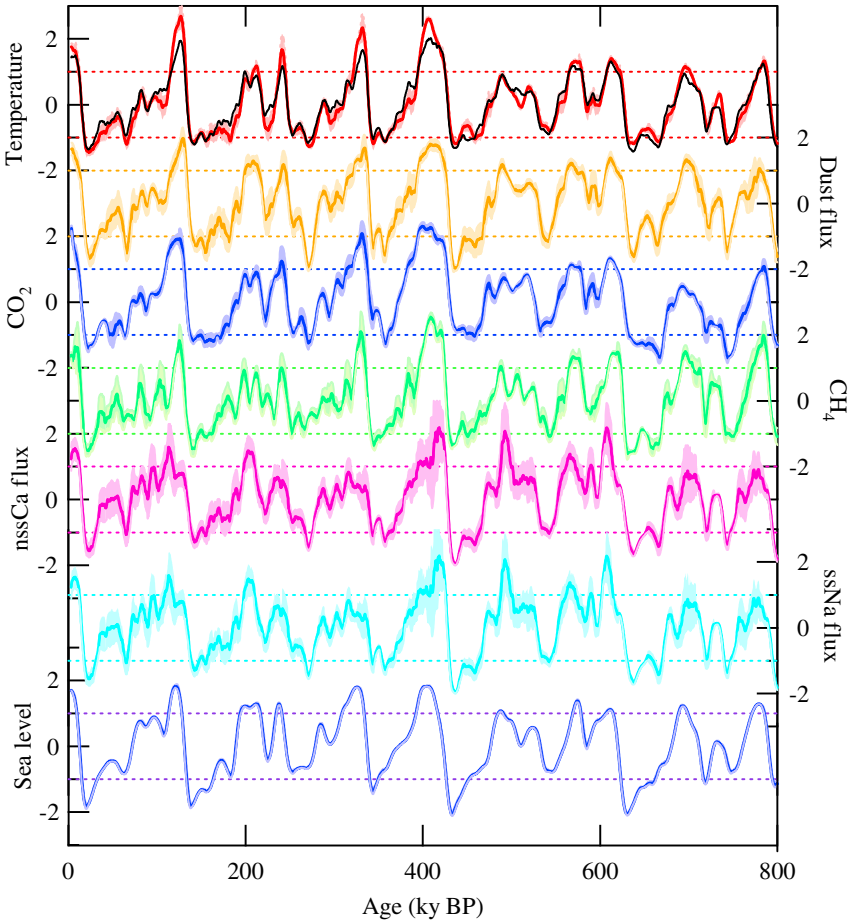

Fig. 2. Climate indices (in standard deviation units) derived from the ice core analyses and from marine sediments. Aerosol records (dust, calcium and sodium flux) were transformed with a logarithm scale to have distributions comparable with other records. All time series were centered, normalised (average over 800 000 years zero, standard deviation 1, positive anomaly during interglacials) and re-sampled with a time resolution of 200 years. In order to analyse the orbital scale features, running averages over 7000 years were performed. The magnitude of suborbital variability (standard deviation within 7000 years) is displayed as the shaded envelop on each record. This apparent suborbital variability is obviously dependent on the initial resolution of the records. Horizontal lines display plus or minus one standard deviation of the full indices. In the upper panel, the temperature index derived from the Jouzel et al., (2007) temperature reconstruction (red) is compared with the average of all the other EDC climate indices displayed below (black line).

2. Changes in evaporation conditions and moisture sources are expected to impact the isotopic composition of the initial water vapour and the isotopic composition of the Antarctic snowfall (Vimeux et al., 2002). Deuterium excess data from EDC have shown that EDC temperature reconstruction is robust with respect to changes in moisture origin over the past climatic cycle (Stenni et al., 2010; Stenni et al., 2001).
3. Changes in precipitation seasonality and/or intermittency are expected to play an important role in the sampling of climate signals recorded in ice cores (Masson-Delmotte et al., 2006b; Timmermann et al., 2009). There is no proxy available to detect past changes in snowfall seasonality. For present day, EDC accumulation is dominated by a few randomly distributed snowfall events (Gallée and Gorodetskaya, 2008). In the Vostok area, a stake network showed that present-day accumulation is regularly distributed year round and mostly (75%) provided by clear sky precipitation (diamond dust) (Ekaykin, 2003). Climate models have been used to quantify the impact of past changes in snowfall seasonality. At the glacial–interglacial scale, modelling studies conducted with isotopic general circulation models support a stable central Antarctic isotope–temperature slope and suggest that glacial–interglacial surface temperature changes based on Antarctic ice core stable isotope records should be valid within ±2 °C (Jouzel et al., 2003; Jouzel et al., 2007).

In order to assess the impact of changes in orbital configuration on precipitation seasonality aspects, we have analysed sensitivity simulations conducted with the IPSL (Institut Pierre Simon Laplace) coupled climate model under pre-industrial boundary conditions and with orbital configurations from present day, 6, 9, 115, 122 and 126 kyr (thousands of years before present) spanning a range of obliquity, precession and eccentricity configurations (Braconnot et al., 2008). For inland Antarctica (above 2500 m elevation), we have calculated the annual mean temperature (average of monthly mean temperatures) and the precipitation weighted temperature from monthly values of temperature and precipitation. The results from this coupled climate model indicate that the absolute value of the seasonal bias (difference between these two annual temperatures) is always lower than 0.5 °C. For 126 kyr, this result is further confirmed by comparable results obtained with three other coupled climate models (see Section 5). A 130 ka transient simulation has recently been conducted with the LOVECLIM model (Timmermann, pers. comm.), forced by astronomical, greenhouse gas, and ice sheet model based estimates of ice sheet topography and albedo. In central Antarctica, the precipitation weighted temperature is on average 1.2 °C above the annual mean surface temperature. Precession appears to modulate this bias by about ±0.75 °C.

Considering uncertainties linked with changes in moisture origin, local elevation, condensation versus surface temperature variations and by snowfall seasonality or intermittency, the

available observations and modelling results briefly summarized here suggest that the uncertainty on EDC temperature reconstruction is within 1–2 °C.

3.2. Relative intensity of glacial and interglacial optima based on multiple EDC proxy records

In this section, we consider the EDC temperature estimates but also the other climate proxies available for the same ice core (EDC dust, non-sea-salt calcium, sea salt sodium, methane and carbon dioxide) and spanning the same time interval (sea level estimates based on marine data). Each record has been re-sampled with a 0.2 kyr time step, centered and normalised to produce indices with a positive sign during interglacials. In order to scrutinize the relative intensity of glacial and interglacial optima at the orbital scale, long-term trends have been extracted using a 7 ky running average (Fig. 2). The level of suborbital variability is indicated by the shading associated with the running standard deviation calculated also over 7 ky. This variability is affected by the initial temporal resolution of the records as discussed in Section 2, but also by the analytical uncertainties and by the actual suborbital climate variability. The comparison of the various indices reveals quite comparable long-term features (for instance, the shape of glacial–interglacial cycles, and the different levels between the "early" 800–400 ky BP and "late" 400–0 ky BP interglacials), but also marked differences (trends and optima during interglacials and glacial inceptions).

Time windows around glacial and interglacial optima were defined to explore more quantitatively the relative intensities of glacial maxima and interglacial maxima in the various proxies (Tables 1a–1c). The relative intensities of these events were given a rank for each of the proxy records considered here. The most intense interglacial and glacial periods can therefore be identified based on a variety of indices, together with the "relative sensitivity" of each proxy regarding its own range of variability between glacial and interglacial extrema.

Changes in sea level or aerosol flux (dust, sodium, calcium) at EDC appear as the indices most sensitive to the variability between glacial maxima. By contrast, EDC δD, EDC temperature, CH_4 and CO_2 seem to saturate during glacial maxima and show limited variability from one glacial maximum to the other. This saturation effect could be real, such as similar glacial Antarctic temperature changes and greenhouse gas concentrations could coincide with different amounts of ice volume on northern hemisphere continents. Alternatively, the saturation effect may be linked with the proxies themselves. Typically, the isotopic composition of glacial cold and dry Antarctica (surrounded and isolated from the rest of the world by an extensive sea ice coverage) may be only weakly affected by different glaciation intensities. With all the proxies considered here, MIS 14 clearly appears as the weakest glacial maximum, while MIS 2, 12 and 16 are the three periods where the strongest glacial maxima occur, although with different relative intensities in the different proxies.

When considering interglacial periods, three indices (sea level, dust and methane) show little dispersion from one interglacial to the other. Due to the minimum ice volume and dust production along interglacials, the fact that these two proxies show little dispersion is not surprising. The EDC methane record clearly shows quite different variability within each interglacial; these differences are clearly imprinted on the high frequency signal (early interglacial overshoots, evolution over the course of interglacial periods) but strongly damped at the orbital scale. By contrast, three indices show large differences from one interglacial period to the other: EDC temperature, sea salt sodium, and CO_2. Temperature and CO_2 clearly show marked changes between the "early" and "late" interglacials. When considering all the proxies, there is no ambiguity that MIS 13 and 17 appear the "weakest" interglacials, while MIS 5.5 and 11 appear as the "strongest" interglacials, but again with different magnitudes depending on the proxies considered.

This section shows that the main features of the glacial–interglacial variations appear common to the various ice core proxies and sea level reconstructions. An interpretation of the results purely based on stable isotopes and EDC temperature would only slightly differ from the signal derived from the other EDC proxy records, for instance regarding the temporal evolution over the course of interglacial periods (Fig. 2).

Table 1a
Comparison of the relative intensities of interglacial periods based on EDC proxy indices (no unit). EDC initial records (converted to a logarithm scale for aerosol data) were centered, reduced (with a positive sign of the index for interglacials), sampled at a 200 year resolution and smoothed over 7000 years in order to analyse "average interglacial intensities" at the orbital scale. The maximum of the smoothed proxy index was identified within large "interglacial" time intervals (end and start dates are given in ky BP) and is reported in the table (red values, the two most intense interglacials for each proxy; blue values, the two less intense interglacials for each proxy). The rank of the interglacials is given for EDC temperature (Jouzel et al., 2007) and also for the averaged index based on the other proxies (dust, sodium, calcium, methane and carbon dioxide). The rank of interglacials is also reported based on the estimate of past ice volume (Bintanja et al., 2005). The "sensitivity" of the various proxies to detect changes in intensity between interglacial periods is estimated using the inter-interglacial index standard deviation σ.

MIS	End	Start	δD	EDC T	Log (dust)	CO_2	CH_4	Log (Na)	Log (Ca)	Rank EDC T	Rank other proxies	Sea level
1	0.0	11.6	1.69	1.76	1.66	2.06	1.65	1.51	1.54	4	4	4
5.5	115.0	132.0	2.70	2.69	1.98	1.93	1.83	3.64	1.44	**1**	**2**	**2**
7.5	233.6	245.6	1.74	1.67	1.18	1.24	1.01	1.99	0.68	5	8	7
9	316.8	335.6	2.46	2.34	1.69	2.08	2.11	2.59	0.81	3	3	3
11	392.0	424.6	2.44	2.61	1.81	2.31	2.55	2.59	2.19	**2**	**1**	**1**
13	470.0	529.6	1.01	0.88	1.19	0.82	1.05	0.54	2.08	**10**	**9**	**10**
15.1	560.0	580.0	1.36	1.32	1.22	1.12	1.35	2.21	1.38	8	6	5
15.5	603.0	628.0	1.45	1.40	1.39	1.32	1.48	1.29	2.18	6	5	**9**
17	680.0	720.0	1.10	1.16	1.34	0.48	1.50	1.24	0.87	**9**	**10**	8
19	769.6	791.6	1.51	1.33	1.06	1.09	2.00	1.78	0.91	7	7	6
σ	–	–	**0.59**	**0.63**	**0.31**	**0.61**	**0.48**	**0.88**	**0.59**	–	–	**0.30**

Table 1b
Same as Table 1a but for the relative intensity of glacial maxima (red, "coolest" glacials; blue, "coldest" glacials).

MIS	End	Start	δD	EDC T	Log (dust)	CO_2	CH_4	Log (Na)	Log (Ca)	Rank EDC T	Rank other proxies	Sea level
2	11.60	35.60	**−1.40**	**−1.45**	−1.68	**−1.40**	**−1.51**	−0.84	−1.56	**9**	6	7
6	135.0	153.0	**−1.07**	**−1.14**	**−1.38**	−1.21	−1.46	−1.01	−1.29	**2**	3	6
8	250.0	278.0	**−1.32**	**−1.27**	**−1.93**	−1.25	**−1.00**	**−1.46**	−1.45	**8**	7	**2**
10	340.0	360.0	−1.15	−1.19	−1.57	−1.27	−1.35	−0.92	**−1.27**	6	4	5
12	425.0	451.0	−1.22	−1.19	**−1.96**	**−0.97**	−1.36	**−1.14**	**−1.95**	5	**9**	**9**
14	528.0	548.0	**−0.87**	**−0.80**	**−1.16**	**−0.88**	**−1.08**	−0.80	**−1.03**	**1**	**1**	**1**
16	621.0	651.0	−1.11	−1.18	−1.62	−1.32	**−1.60**	−1.13	−1.66	4	**8**	**8**
18	742.0	755.6	−1.15	**−1.14**	−1.47	**−1.69**	−1.08	**−0.67**	−1.36	3	**2**	3
20	798.8	801.6	−1.26	−1.19	−1.68	−1.32	−1.11	**−0.62**	**−1.86**	7	5	4
σ	–	–	**0.15**	**0.17**	**0.25**	**0.24**	**0.22**	**0.26**	**0.29**	–	–	**0.55**

4. Links between changes in radiative forcing and climate

In this section, we now discuss the links between EDC temperature and climate forcings using different approaches. At the local scale, radiative forcings involve changes in obliquity (which affects annual mean insolation) (Section 4.1) and greenhouse gas concentrations (which affects the infra-red loss) (Section 4.2.1). We analyse in Section 4.2.2 the links between EDC temperature and local radiative forcings caused by obliquity and greenhouse gas concentrations.

In a second step, we then use climate models to explore the relationships between central Antarctic and global temperature and to estimate past changes in global temperature. At the global scale, changes in orbital parameters have a negligible impact, and changes in radiative forcing mostly result from changes in greenhouse gas concentration and ice sheet albedo. We compare the global mean temperature *calculated* with a constant climate sensitivity in response to past changes in ice sheet and greenhouse gas radiative forcings, with the global mean temperature *estimated* from EDC temperature and other paleoclimatic records.

4.1. Orbital frequencies in EDC temperature reconstructions

We now examine the power spectrum of EDC temperature variations at the orbital scale. Note that the EDC3 age scale is independent of the orbital properties of EDC deuterium data (see Section 2). Earlier studies (EPICA-Community-Members, 2004; Masson-Delmotte et al., 2006a; Jouzel et al., 2007) have revealed (1) that EDC temperature exhibits power spectrum in the 100 ky, 40 kyr and 20 ky periodicity ranges, with a strong obliquity signal, and (2) that the imprints of both precession and obliquity increase from past to present. Here we discuss how the sea water isotopic composition and the elevation corrections influence EDC temperature power spectrum.

Fig. 3 displays the spectral amplitude of the initial deuterium profile and of two temperature estimates (conventional method; elevation correction) for three time intervals (0–800 ka; 0–400 ka and 400–800 ka). Over the full EDC profile (800 ka), the sea water isotopic composition and the elevation corrections have no detectable impacts on the spectral amplitudes. All the estimates of EDC temperature show a strong obliquity signal, and an increasing amplitude of the precession and obliquity periodicities from the past (400–800 ka) to the present (0–400 ka). We conclude that the increasingly strong obliquity signature in the EDC temperature is not an artefact of biases due to corrections linked with sea water isotopic composition or EDC elevation changes. The increasing intensity of interglacial periods from past to present was suggested to be linked with the long-term increase in obliquity amplitude (Jouzel et al., 2007).

As changes in obliquity have a direct impact on Antarctic annual mean insolation (6 W m^{-2} of top of atmosphere local annual mean insolation per degree obliquity), they have to be included in the analysis of the factors driving the *local* radiative forcing (see Section 4.2.2). Note however that the observed 5 ky lag between EDC temperature and obliquity (Jouzel et al., 2007) shows that complex feedbacks involving slow climate components are at play in addition to a fast response to local insolation.

4.2. Relationships between EDC temperature and local radiative forcings

4.2.1. Estimating local greenhouse gas radiative forcings over the past 800 000 years

The greenhouse gas radiative forcing can be estimated at the global scale using Eq. (1). However, the local impact of changes in greenhouse gas concentrations depends on the vertical temperature and humidity profiles. The central Antarctic radiative budget is dominated by the infra-red loss and its interplay with the strong thermal inversion (Connolley, 1996) – without this inversion, the surface long-wave net radiative loss would be increased by 18% (summer) to 30% (winter). In order to roughly quantify the local radiative perturbations caused by changes in orbital parameters and atmospheric greenhouse gas concentrations, taking into account the particularities of the Antarctic albedo and atmospheric

Table 1c
Summary of the results of Tables 1a and 1b.

	Least sensitive proxies	Most sensitive proxies	Coldest MIS (no intensity ranking)	Warmest MIS (no intensity ranking)
Variability between glacial maxima	δD, EDC T CH_4, CO_2	Sea level Aerosols (dust, Na, Ca)	MIS 2, 12, 16	MIS 14
Variability between interglacial maxima	Sea level Dust, CH_4	δD, EDC T Na, CO_2	MIS 13, 17	MIS 5.5, 11

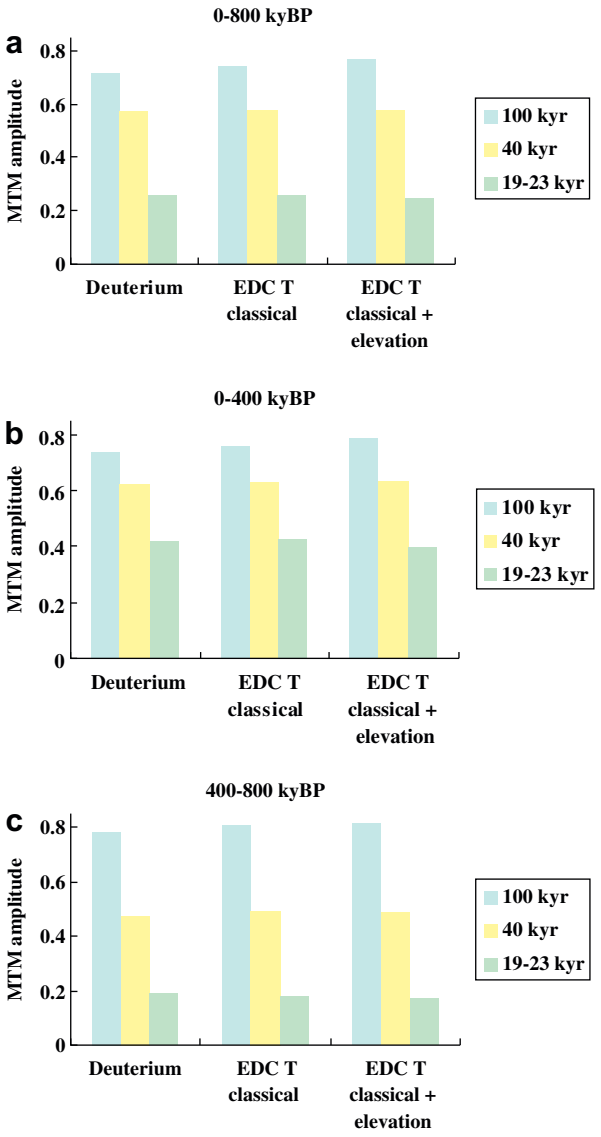

Fig. 3. Multi-Taper Method amplitude in the orbital bands (blue, 75–130 kyr range; yellow, 33–50 kyr range; green, 17–27 kyr range) obtained for EDC δD and for two different temperature reconstructions, either using the conventional method after correction for sea water isotopic composition (Tsite conventional), or including also an altitude correction (Jouzel et al., 2007). Analyses have been performed on three different time intervals: 0–800 ky BP (a); 0–400 ky BP (b) and 400–800 ka BP (c).

structure, we use here a 1D radiative model (Li and Treut, 1992). Changes in radiative fluxes are calculated using an iterative adjustment of stratospheric temperature, in order to represent all the non-explicitly resolved processes (apart from radiation) that act to maintain the energetic budget of the atmosphere. While the model does not correctly represent the adjustments of the vertical temperature profile of the atmosphere, it enables the diagnosis of changes in radiative fluxes due to specific perturbations. All our calculations have been conducted under clear sky conditions, following earlier studies (Huybers and Denton, 2008). The model requires as inputs: orbital parameters (to calculate local insolation), vertical temperature, relative humidity, ozone concentration profiles (kept at pre-industrial values), and concentrations of greenhouse gases.

The surface albedo depends on the zenithal angle and varies between ~0.82 and 0.92. The local net short-wave radiation balance perturbation by changes in eccentricity is small (~0.6 W m^{-2}). Changes in precession can modify the summer net short-wave radiation balance by up to ~4 W m^{-2}. Obliquity effects alter the duration of seasons (Huybers and Denton, 2008) and the annual mean net surface short-wave radiation budget (by ~2 W m^{-2}).

The impact of greenhouse gas concentrations depends on the vertical temperature and specific humidity profiles. We have considered present-day December and August vertical profiles from ECMWF analyses (Chevallier, pers. comm.). We have performed sensitivity tests to explore the importance of the mean state of the local atmosphere with respect to the radiative forcing caused by greenhouse gas concentration changes. For these sensitivity tests, we have shifted the temperature profile by assuming a −10 °C or +5 °C surface temperature change, and kept the same inversion strength (a ratio of 0.67 between surface and inversion temperatures in °C) as today (Connolley, 1996). This range of surface temperature changes is directly inspired by the EDC T derived from the ice core data over 800 ka. Tests have also been conducted by changing the vertical profile of specific humidity using the saturation vapour pressure dependency on temperature. This hypothesis is also used for modelling the ice core accumulation rates.

Changing the greenhouse gas concentration from pre-industrial to LGM levels induces a local radiative forcing of 1–2 W m^{-2} (see Fig. 4), representing a local perturbation of about 2% of the net long-wave radiative balance. Results obtained from the LGM simulations run with the coupled IPSL model are in excellent agreement with this 1D estimate (Pol et al., 2008). Both for decreased or increased ($2 \times CO_2$) greenhouse gas levels, a weaker (respectively stronger) local radiative forcing is calculated at cold (respectively warm) mean temperatures (Fig. 4). The LGM radiative forcing perturbation is enhanced by 15% (summer) to 30% (winter) when taking into account the adjustment of the vertical humidity profile expected from a prescribed 10 °C cooling. The positive water vapour feedback seems however smaller under warm conditions (+5 °C sensitivity test).

Altogether, due to thermal inversion, the local greenhouse gas radiative forcing is systematically smaller than the global radiative forcing estimated with Eqs. (1) and (2) (see Section 2) and this difference is enhanced for cold climates. The local calculation gives a result which is proportional to the global estimate from Eq. (1). Due to uncertainties on past vertical profiles of temperature and humidity, we use in the Section 4.2.2 the global greenhouse gas radiative forcing calculation using Eqs. (1) and (2).

4.2.2. Relationships between past EDC temperature and past local radiative forcings

At the local scale, we need to account for changes in annual mean insolation (proportional to obliquity) and changes in greenhouse gas radiative forcing. Fig. 5a displays the greenhouse gas radiative forcing of EDC CH_4 and CO_2, calculated – at the global scale – from Eqs. (1) and (2). In principle, one should use the local Antarctic radiative forcing due to changes in greenhouse gas concentrations, but this would add uncertainties due to the interplay with local temperature and humidity vertical profiles as discussed in Section 4.2.1. The shape of this curve is dominated by the impact of CO_2 fluctuations. Its most remarkable feature is a low radiative forcing in the oldest part of the time series (from MIS 16 to MIS 19, prior to 600 ky). This effect was previously described based on CO_2 concentration data and was suggested to arise from long-term (several 100 ky) changes in the carbon cycle in relationship with geological processes (Lüthi et al., 2008). Fig. 5a also displays EDC T estimated after elevation correction (see Section 3.1) (Jouzel et al., 2007) and obliquity, which is the main driver of past changes in local annual mean incoming insolation. The lags between EDC T and greenhouse gas radiative forcing remain uncertain within

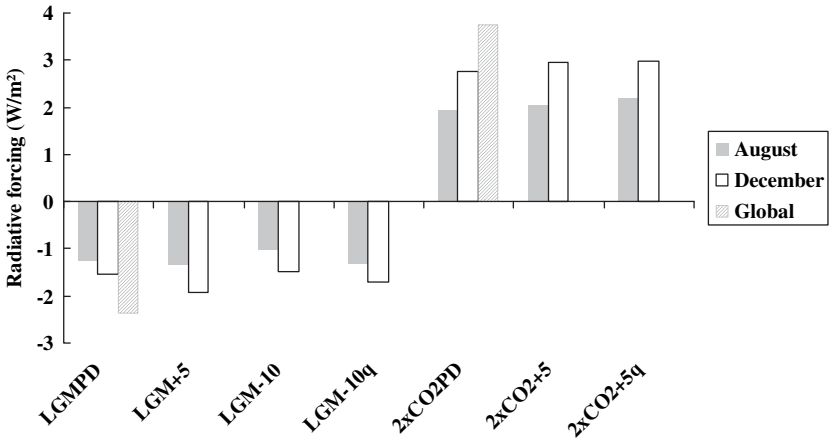

Fig. 4. EDC radiative forcing calculations. The radiative budgets are calculated with a 1D radiative transfer model forced by prescribed vertical profiles of temperature and specific humidity, and different concentrations in greenhouse gases (pre-industrial, 280 ppm of CO_2, 580 ppb of CH_4, 270 ppb of N_2O; LGM, 180 ppm of CO_2, 390 ppb of CH_4, 220 ppb of N_2O; $2 \times CO_2$, 560 ppm, other gases at their pre-industrial levels). A fixed pre-industrial ozone concentration profile is used. The present-day vertical temperature profiles are obtained from ECMWF analyses for December and August. Sensitivity tests are conducted by shifting the surface temperature by −10 or +5 °C, assuming constant inversion strength, and by calculating associated humidity (q) profiles (using the saturation vapour pressure–temperature relationship). Vertical bars display changes in radiative forcing changes between pre-industrial greenhouse gas concentrations and LGM or $2 \times CO_2$ greenhouse gas concentrations, for different hypotheses of vertical temperature and humidity profiles (PD, present day; +5 or −10 °C perturbations; "q" indicates a calculation of specific humidity feedback) and for two seasons (August, grey and December, white). For comparison, global annual radiative forcing calculations from Eq. (1) are displayed (shaded bars).

a few centuries due to gas age–ice age differences (Dreyfus et al., 2010).

Fig. 5b displays the relationship between EDC T and the greenhouse gas radiative forcing. The colour scale is used to show the temporal evolution, ranging from blue (800 ky BP) to red (present day), as indicated on the EDC T profile (Fig. 5a). The relationship between EDC T and greenhouse radiative forcing exhibits a crescent (convex) shape. During glacial minima, the slope between temperature and radiative forcing is very small, while it appears larger for the warmest interglacials. The relationship is not symmetric between glacial inceptions and terminations. It exhibits a hysteresis behaviour with values above the linear fit for terminations and below the linear fit for inceptions. Interglacial periods exhibit a complete decoupling of the greenhouse gas radiative forcing and EDC T (Fig. 5a). As a first approximation, we can use a linear relationship between EDC T and radiative forcing, with a slope of 3.9 °C per W m^{-2} ($R^2 = 0.80$), or a parabolic fit ($R^2 = 0.82$) (Fig. 5b). An F-test conducted on the residuals confirms lower unexplained variance for the parabolic fit than for the linear fit ($p = 2 \times 10^{-5}$). The "crescent" (convex) shape is robust with respect to the method used to estimate the local greenhouse gas radiative forcing (using Eqs. (1) and (2)) or more precise local radiative calculations leading to a smaller radiative forcing under colder conditions, see Section 4.2.1.

While EDC T shows a strong obliquity signal (see Section 4.1), the linear relationship between EDC T and obliquity is small but significant (95% confidence level), with a slope of 1 °C per degree obliquity ($R^2 = 0.1$). Note that a maximum R^2 of 0.2 is reached using a lag of 5 ky, leading to a slope of 2.1 °C per degree obliquity. Here, we explore the impact of instantaneous annual mean radiative forcings on Antarctic temperature and therefore ignore this lag. A multiple linear regression leads to a reconstructed EDC T which captures 82% of EDC T variance (93% through changes in greenhouse gas radiative forcing and 7% due to changes in obliquity). In order to identify the part of EDC T which cannot be explained by a simple linear response to changes in greenhouse gas radiative forcing and in-phase obliquity, we have displayed the residual of EDC T (grey line, Fig. 5a). The magnitude and shape of this residual is unchanged when considering obliquity or not, or when considering a linear or parabolic link with greenhouse gas radiative forcing, or when using Eqs. (1) and (2) or local estimates of greenhouse gas radiative forcing (see Section 4.2.1). The result is not sensitive to the corrections for past changes in EDC elevation. A part of the sharp variations of this residual temperature cannot be discussed as they arise from the phase lags between temperature and greenhouse gas variations during terminations or inceptions. The millennial variability reflects the Antarctic Isotopic Maxima (AIM), which are the Antarctic temperature counter-part of Dansgaard–Oeschger variability (EPICA-Community-Members, 2006; Jouzel et al., 2007; Loulergue et al., 2008). AIM events are understood to be driven by reorganisations in meridional oceanic circulation (Stocker and Johnsen, 2003) and correlate with parallel millennial variations in atmospheric CO_2 concentration, reaching ~20 ppmv (Ahn and Brook, 2008) (Schmittner and Galbraith, 2008). These millennial CO_2 variations are not fully resolved in the current Vostok and EDC low resolution profiles. We therefore focus on the multi-millenial variations, highlighted in red using an orbital band Gaussian pass filter (see caption of Fig. 5a).

First, this residual reveals a long-term trend. From about 800 ky BP to about 380 ky BP, the EDC temperature residual shows a slow decreasing trend, followed by a slow increasing trend towards the present day. These slow trends were not obvious in the profiles of greenhouse gas concentrations, radiative forcing, or the initial EDC temperature. This trend cannot be explained by the current understanding of past changes in ice sheet elevation (Pollard and DeConto, 2009). This result suggests that long-term processes alter the coupling between greenhouse radiative forcing and temperature. In other words, the response of Antarctic temperature to changes in radiative forcing may vary over a time scale of ~400 ky. The cause for such long-term fluctuations remains to be understood.

Secondly, this residual reveals a strong obliquity component, which can be seen from the comparison of its orbital component (red line) with the fluctuations of obliquity (yellow line) (Fig. 5a). Most of the obliquity component in EDC T is not due to the local and instantaneous response to Antarctic insolation change (or to the obliquity component of the greenhouse gas radiative forcing) but to a delayed response (with a lag of 5 ky with respect to obliquity). There is therefore a strong obliquity component in the residual. The coherency of the residual with obliquity is minimal for the period

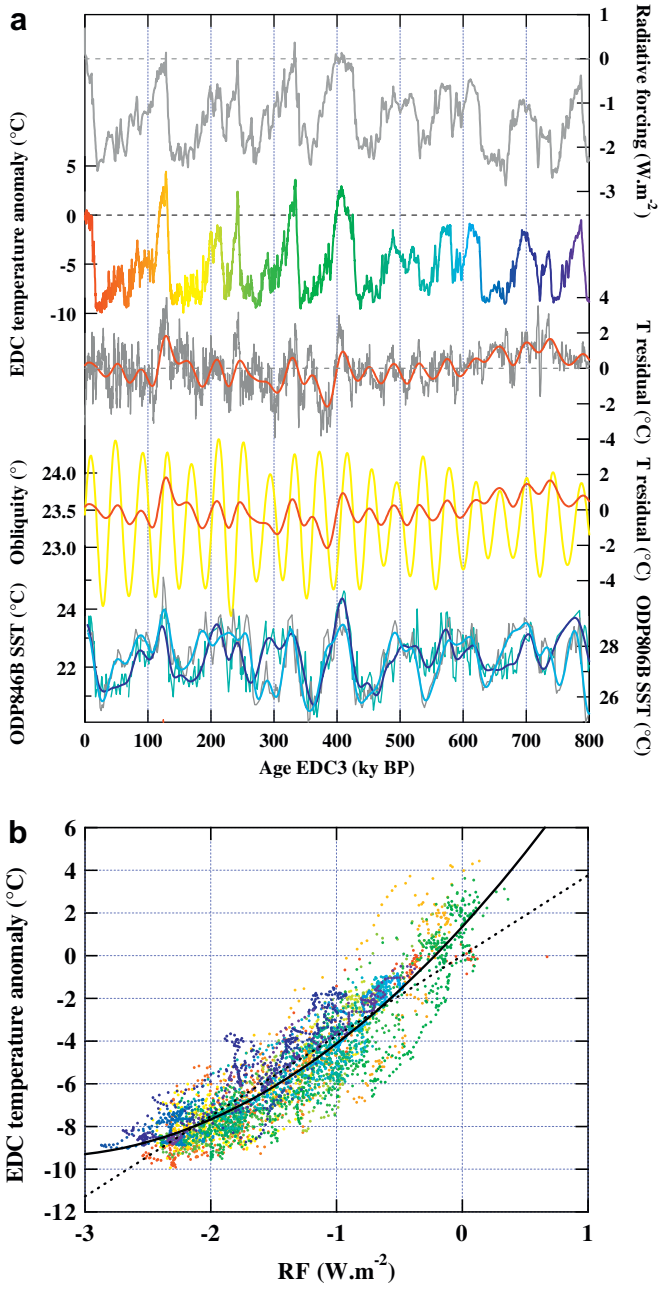

Fig. 5. (a). Change in radiative forcing due to CO_2 and CH_4 calculated using Vostok and EDC data (Petit et al., 1999; Loulergue et al., 2008; Lüthi et al., 2008) using the formula of Joos (2005) (top panel, grey line). EDC temperature with elevation correction (Jouzel et al., 2007) (colour scale reflecting the temporal evolution from past to present, blue to red). A regression is calculated between EDC T and radiative forcing (Fig. 5a). The residual part of EDC temperature that cannot be explained by a multiple linear model considering greenhouse gas radiative forcing and obliquity (dark grey, using a parabolic regression; red line, orbital long-term component of the regression residual). This orbital component (red line) is superimposed on the obliquity fluctuations (yellow line). SST records from the Pacific Ocean are displayed in the lowest panel, based on alkenones for ODP846B (thin grey line, original data; thick light blue, low pass filter) (Lawrence et al., 2006) and on Mg/Ca for ODP806B (thin light blue line, original data; thick dark blue, low pass filter) (Medina-Elizalde and Lea, 2005). (b). Change in EDC temperature (Jouzel et al., 2007) (vertical axis, °C) as a function of the radiative forcing due to CO_2 and CH_4 calculated using Vostok and EDC data (Petit et al., 1999; Loulergue et al., 2008; Lüthi et al., 2008) using the formula of Joos (2005) (Eqs. (1) and (2)). The colour scale reflects the temporal evolution from past to present, blue to red as in Fig. 6b. Linear (dashed line) and parabolic (solid black line) regressions are displayed.

between 350 and 400 ky, a period poorly constrained in the EDC3 age scale (Dreyfus et al., 2007; Parrenin et al., 2007a), questioning the accuracy of the EDC3 age scale for MIS 10–12. This analysis reveals that the large signature of obliquity in EDC temperature (Jouzel et al., 2007) cannot solely be attributed to the obliquity component of the greenhouse gas radiative forcing or to instantaneous local incoming solar radiation. The fact that the obliquity signal is in phase in equatorial Pacific sea surface temperature records (Medina-Elizalde and Lea, 2005; Lawrence et al., 2006) and in Antarctica suggests coupling mechanisms between low and high latitudes, as also observed at the multi-decadal time scale (Ekaykin et al., 2004). There are also long-term trends in the equatorial Pacific sea surface temperatures between 800 and 400 ky BP which suggest that this low–high latitude coupling may also be at play on longer time scales (Fig. 5a).

While levels of greenhouse gas radiative forcing and obliquity can account for different "mean levels" of interglacials, this is not the case for the EDC T evolution over the course of interglacial periods. Early interglacial optima cannot be explained by a simple response to changes in local radiative forcings.

4.3. Relationships between EDC temperature and global temperature

One may want to use EDC greenhouse gas radiative forcings, infer global temperature from EDC temperature, and finally discuss global climate sensitivity based on glacial–interglacial changes, following the pioneer approach conducted for Vostok (Genthon et al., 1987). Based on Last Glacial Maximum (LGM) PMIP (Paleoclimate Modelling Intercomparison Project), climate model simulations, the glacial–interglacial change in central Antarctic temperature appears to be linked with global temperature change, with an amplifying factor of ~2 (Masson-Delmotte et al., 2006a) (Fig. 6). Under present-day boundary conditions, and in response to increased CO_2 levels, coupled climate models also exhibit a linear relationship between central Antarctic and global temperature changes (Fig. 6), albeit with a slope of ~1.2. A 130 ka simulation conducted with the intermediate complexity model LOVECLIM (see Section 3.1) also shows strong correlation between Antarctic and global temperature, with a slope of ~2 (Timmermann, pers. comm.).

This result can be compared with modelling studies conducted with different versions of the same climate model with different equilibrium CO_2 sensitivities, mostly comparing their results for the LGM and for future climate change. An intermediate complexity climate model (Schneider von Deimling et al., 2006) showed an LGM Antarctic cooling of 2.5 °C per °C of climate sensitivity (therefore 7.5 °C for the most plausible 3 °C equilibrium sensitivity). Studies with a general circulation model (Hargreaves et al., 2007) also highlighted a strong link between the model sensitivity and its Antarctic temperature response. Finally a linear relationship between LGM Antarctic cooling and CO_2-induced Antarctic warming was demonstrated with four coupled climate models (Crucifix, 2006) (see his Fig. 2).

State-of-the-art PMIP2 (Paleoclimate Modelling Intercomparison Project, Phase 2) coupled climate models simulate a global LGM cooling of 4.6 ± 0.9 °C and a central Antarctic annual mean surface air temperature changes of 8.8 ± 3.6 °C (Fig. 6). The simulated Antarctic temperature change seems at first sight in very good agreement with EDC T reconstruction (Fig. 1). However, half of the simulated glacial–interglacial Antarctic temperature magnitude is an artefact of the prescribed PMIP2 glacial boundary conditions. Whereas all ice sheet glaciological models suggest that the LGM topography was ~100–200 m lower than at present in central East Antarctica, because of the lower glacial accumulation (see Section

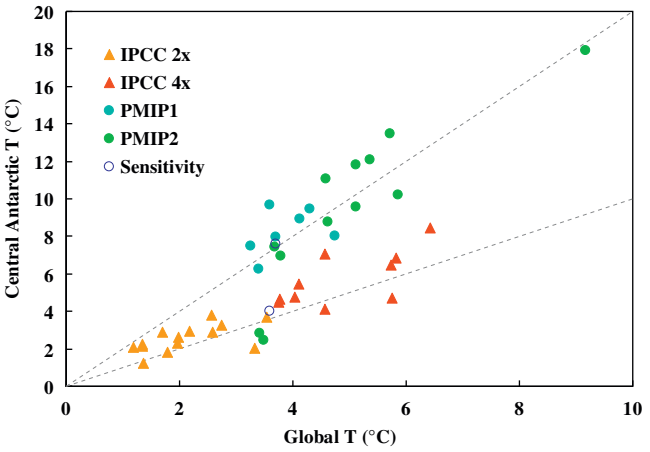

Fig. 6. Comparison between Central Antarctic (area above 2500 m elevation) and global surface air temperature changes simulated by coupled climate models in response to sensitivity simulations to CO_2 increase (orange, CMIP $2\times CO_2$ minus control; red, $4\times CO_2$ minus control) and in response to Last Glacial Maximum boundary conditions (in blue, control minus PMIP1; in green, control minus PMIP2 LGM boundary conditions). Datasets for CMIP simulations are similar to those inform earlier studies (Masson-Delmotte et al., 2006b). Datasets for PMIP2 simulations have been updated from these references to include 5 more model results (PMIP database http://pmip2.lsce.ipsl.fr/on date of November 25th, 2008). Sensitivity tests are LGM simulations conducted with the LMDZ model with ICEG5 ice sheet topography (upper circle) and with the modern Antarctic topography (lower circle). The dashed lines show slopes of 1:1 and 2:1.

3.1 and Fig. 1), the LGM ICE5G topography (Peltier, 2004) interpolated in PMIP simulations is ~400 m above present day in central Antarctica. Using the modern spatial altitude–surface air temperature gradient of ~10 °C per km, we can roughly estimate that the prescribed topography should account for a ~4 °C Antarctic cooling at LGM, almost half of the simulated magnitude.

A specific sensitivity study has been conducted with the LMDz atmospheric general circulation model (Hourdin et al., 2006). With this model, three different LGM simulations were run. All simulations include changes in orbital parameters and greenhouse gas concentrations following PMIP recommendations (Joussaume and Taylor, 1995). The first one (CLIMAP-ICE5G) is a conventional PMIP1 type simulation (Joussaume and Taylor, 1995) using CLIMAP SST (CLIMAP, 1981) and ICE5G ice sheets (Peltier, 2004). The second simulation (GERSONDE-ICE5G) is a sensitivity test to the southern ocean surface boundary conditions performed using new reconstructions (Gersonde et al., 2005). The third simulation (GERSONDE-MODERN) is a sensitivity test to the Antarctic ice sheet topography performed using the present-day Antarctic ice sheet with the same ocean surface data (Gersonde et al., 2005). These simulations show no significant impacts of southern boundary conditions on global mean and Antarctic temperature changes (not shown), coherent with limited impacts of austral sea ice albedo found in PMIP2 simulations at the LGM (Braconnot et al., 2007). The comparison between annual mean temperature and precipitation weighted temperature changes confirms earlier AGCM studies suggesting limited (<1.3 °C) LGM central Antarctic seasonality effects (Krinner et al., 1997; Krinner and Werner, 2003; Masson-Delmotte et al., 2006a). By contrast, the impact of changes in ice sheet topography is striking. The ICE5G change in topography does not affect the seasonality of precipitation but accounts for a simulated temperature change at Dome C of 3.6 °C (blue circles, Fig. 6), almost half of the LGM-control magnitude. This sensitivity study confirms our initial prediction that almost half of the PMIP simulated glacial–interglacial central Antarctic temperature may be an artefact of the prescribed LGM ice sheet topography (Masson-Delmotte et al., 2006a).

The uncertainty linked with the prescribed PMIP2 Antarctic ice sheet topography limits the model-data comparison, but most model simulations (Fig. 4) clearly show a strong link between the simulated Antarctic and the simulated global mean temperature both for past and future climate boundary conditions. Following earlier studies (Lorius et al., 1990a; Hansen et al., 2008), we assume that past global mean temperature changes can be estimated using past EDC temperature changes. Our fixed point is the LGM for which global ocean temperature databases and climate model simulations are available (Otto-Bliesner, 2009).

We therefore use a slope of 1/2 to estimate past changes in global temperature from changes in EDC T (Fig. 7). This scaling may be inappropriate for interglacial periods, for which increased CO_2 climate change simulations suggest a slope of 1/1.2 (Fig. 6). This scaling is also problematic for millennial bipolar seesaw events such as Antarctic Isotopic Maxima (EPICA-Community-Members, 2006). Due to the uncertainties on EDC T reconstructions (typically 2 °C), the magnitude of millennial variability (typically 2 °C), and the uncertainty on the slope between Antarctic and global temperature (between 1.16 for future climate and 2 for LGM), we estimate an uncertainty of about 1–2 °C on the reconstructed global mean temperature (1 °C light red shading, Fig. 7).

There is no available global synthesis of temperature records spanning the past 800 000 years from other latitudes. Other estimates of past global temperature changes have been previously published using deep ocean temperature (Zachos et al., 2001; Bintanja et al., 2005) or tropical Sea Surface Temperature (SST) records (Lea, 2004; Medina-Elizalde and Lea, 2005; Hansen et al., 2008) also scaled for the LGM with a slope of 2/3 (see their comparison on Fig. 7). Detailed comparisons are limited by the resolutions of the records (much higher for EDC), age scale and lags uncertainties. Each of these estimates is of course biased by the proxy records potentially affected by seasonality effects and by the

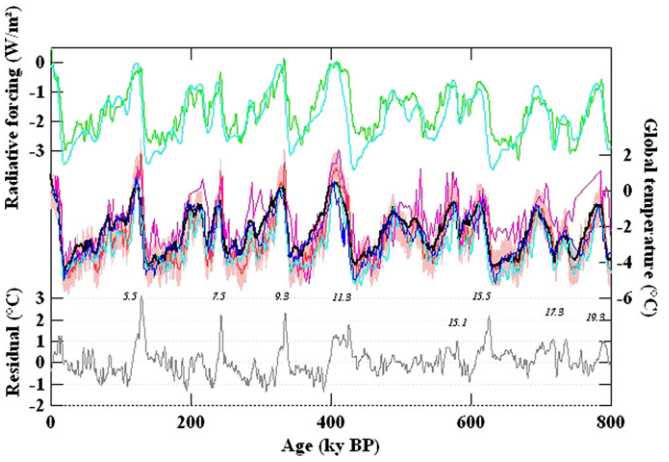

Fig. 7. Calculation of global radiative forcings (Hansen et al., 2008) associated with slow feedback processes involving past changes in carbon cycle (global greenhouse gas concentrations using only continuous records of EDC and Vostok CO_2 and CH_4) (green) and in ice sheet extent, deriving ice sheet extent as a function of an estimate of northern and southern hemisphere ice volume using global ice volume estimates from Bintanja et al. (2005) (in light blue). The global temperature change is estimated using either a ratio of 1/2 with respect to EDC temperature (red, with a ±1 °C uncertainty shading), a ratio of 2/3 from equatorial Pacific SST (Medina-Elizalde and Lea, 2005) (pink) or deep ocean temperature (blue) (Zachos et al., 2001) (light blue) (Bintanja et al., 2005). The global temperature change is calculated using the past ice sheet albedo and greenhouse gas radiative forcings and the fast feedback global temperature sensitivity of 0.75 °C per W m^{-2} (Hansen et al., 2008) (black). The residual between the estimated global temperature using EDC temperature and the modelled global temperature is displayed in grey. Marine Isotopic Stages associated with strong residuals are displayed.

different mechanisms linking local and global temperature (Bintanja and Van de Wal, 2008; Sosdian and Rosenthal, 2009). The comparison of the various methods shows that they share common features (amplitude of the glacial–interglacial changes, different intensities of early versus late interglacials) while they exhibit significant differences, especially regarding the temperature evolution within an interglacial period. We note that the estimate based on deep sea temperature shows ~0.5–1 °C more pronounced Lateglacial maxima than those based on EDC T (Fig. 7). The global temperature estimate based on EDC T shows a ~0.5–1 °C stronger cooling during glacial inceptions than the estimate based on tropical SST; this is probably due to the different timing of glacial inception at different latitudes (see for instance Vimeux et al., 1999).

4.4. Modelled global temperature change and relevance for climate sensitivity

Past changes in *global* radiative forcings mainly arise from past changes in greenhouse gas concentrations but also from changes in ice sheet albedo. The greenhouse gas radiative forcing can be estimated using published formulas (Eq. (1)). One uncertainty arises from the interplay of N_2O forcing and the indirect effect of CH_4 on tropospheric ozone and stratospheric water vapour (Hansen et al., 2008). The glacial–interglacial greenhouse gas forcing reaches about 3 W m^{-2}, 3/4 of which is caused by CO_2. Past changes in global radiative forcings due to the growth and decay of ice sheets can also be estimated using estimates of ice volume changes based on marine benthic stacks (Bintanja et al., 2005). The albedo of the ice sheets is expected to be proportional to their area, which, in circle symmetric parabolic ice sheet models, is expected to vary to the 4/5 power of their volume. The change in global ice sheet albedo radiative forcing also reaches about 3 W m^{-2} at the glacial–interglacial scale (IPCC, 2007). In theory, one should take into account the latitudinal expansion of the ice sheets and the actual changes in insolation as a function of the season and the latitude to calculate more accurately the ice sheet radiative forcing (Köhler et al., 2010). Changes in topography (land sea mask) and in vegetation are expected to add ~0.5 W m^{-2} of additional radiative forcing (IPCC, 2007). Another uncertainty arises from the changes in snow cover (with possible impacts on snow-covered ice sheet albedo), atmospheric aerosol and dust loading between glacials and interglacials (IPCC, 2007), all fast feedback processes which are discussed in detail in another paper from this issue (Köhler et al., 2010).

Here, we consider separately global radiative perturbations resulting from long-term readjustments in the climate system (carbon cycle, ice sheets) and those resulting from faster components of the system (snow, sea ice, vegetation, dust). We consider that the reactions of these fast components are part of the climate feedbacks (Lorius et al., 1990b; Hansen et al., 2008) which also involve changes in the atmospheric temperature, water vapour and cloud distributions (Köhler et al., 2010). Regarding fast versus slow feedback processes, it remains difficult to determine what is the sequence of events triggered by orbital forcing. Available data suggest that terminations are associated with first an increase in Antarctic temperature, followed after several centuries by an increase in greenhouse gases (Fischer et al., 1999; Caillon et al., 2003). The phase lag between ice volume changes, greenhouse gas changes and EDC/global temperature changes remains uncertain (Loulergue et al., 2007). The apparent sequences of events do not only reflect the response of climate to orbital forcing but can also be affected by millennial events (with contrasted north/south signatures in temperature) (Wolff et al., 2009). It was recently considered (Hansen et al., 2008) that changes in ice sheet albedo were the single radiative forcing, considering changes in greenhouse gas concentration as a slow feedback, and therefore introducing fast and slow climate sensitivity parameters. Regarding the relative importance of these "fast" feedbacks (snow cover, sea ice, vegetation, mineral dust in the atmosphere), we refer the reader to another paper from the same issue (Köhler et al., 2010).

We therefore consider the global radiative forcings due to only ice sheet albedo and greenhouse gas concentrations (Fig. 7). The global temperature change can then be estimated using the total global radiative forcings (from the ice sheet albedo effect and greenhouse gas as derived from the ice cores) assuming a constant fast feedback climate sensitivity of 0.75 °C per W m^{-2} (IPCC, 2007) (black line, Fig. 7).

The comparison between our very simple estimate of past changes in global temperature and different estimates of global temperature (Fig. 7) is surprisingly efficient. It is striking that many features of the temperature variations can be explained with this simple approach, such as the relative magnitudes of glacial–interglacial changes and the lukewarm early interglacial periods. Assuming a constant climate sensitivity leads to a better fit with the oldest climatic cycles than for the most recent climatic cycles (which have stronger magnitudes): the observed slope between EDC-derived global mean temperature and radiative forcing is 0.76 ± 0.01 °C per W m^{-2} for the time interval from 440 to 800 ka, but 0.86 ± 0.01 °C from 0 to 440 ka. This observation opens several questions, such as the stability of the climate sensitivity under different background climate conditions. Modelling studies conducted with general circulation models (Hargreaves et al., 2007; Hansen et al., 2008) (Fig. S2) argue for a weaker global climate sensitivity under glacial conditions than for future increased CO_2, possibly due to water vapour and ice cloud feedbacks.

It is also striking that the shapes of the various EDC interglacial periods cannot be explained by our approach. In order to highlight the mismatch between the modelled response to the global radiative forcing and the EDC-derived global temperature estimate, we have represented the residual between these two datasets (grey line, Fig. 7). This residual remains mostly within our uncertainty (±1 °C). Two remarkable features appear: (i) interglacial optima which cannot be accounted for by changes in global radiative forcings, and (ii) long-term trends. The long-term trends probably reflect the high latitude bias of EDC T which shows faster glacial inceptions than tropical records (see Fig. 7 and Section 4.3), and the obliquity signal which is more strongly imprinted at high than low latitudes. Regarding interglacial optima, their timing may be specific to Antarctica (see the discussion of Holocene optima in IPCC, 2007, Chapter 6, Fig. 6.9) and the evolution of global temperature along interglacial periods remains highly uncertain. With two different methods (see Section 4.3), we have clearly shown that these optima cannot be explained by changes in local or global radiative forcing linked with greenhouse gas concentrations and northern hemisphere ice sheets. In the Section 5, we focus on these early interglacial optima.

5. Discussion of Antarctic interglacial optima

We focus here on MIS 5.5, which appears as an exceptional interglacial period in EDC temperature with the highest temperature of the past 800 ka. It is also exceptional with respect to the residual between EDC temperature and the greenhouse gas radiative forcing (Fig. 6b). Here we use climate models to explore climate feedbacks involved in the simulated response to MIS 5.5 orbital forcing and compare the simulated polar responses in the northern and southern hemispheres (Greenland and Antarctica).

Greenland ice cores cover parts of MIS 5.5, back to ~123 ky BP in the bottom part of the unperturbed NGRIP ice core (NorthGRIP-Community-Members, 2004; Landais et al., 2005) and in pieces of the disturbed parts of the GRIP and GISP2 ice cores (Landais et al., 2003). The 3‰ enhanced Greenland ice core $\delta^{18}O$ suggest that Greenland temperature was ~5 °C above present day, with the usual caveats and uncertainties regarding changes in snowfall seasonality and their impact on the temperature estimates (Masson-Delmotte et al., 2005; Masson-Delmotte et al., 2006b). Syntheses of other terrestrial and marine proxy records support a 3–5 °C MIS 5.5 summer warming in the Arctic (Otto-Bliesner et al., 2006).

In Dome C, Vostok (Petit et al., 1999), Dome Fuji (Watanabe et al., 2003) and Dronning Maud Land (EPICA-Community-Members, 2006), the East Antarctic temperature derived from stable isotopes shows a first transient optimum, reaching up to ~5 °C above present day, followed by a multi-millennial plateau associated with temperatures ~2 °C above present day. Unfortunately, no other temperature reconstruction method has yet been found to confirm these magnitudes. Independent hints that MIS 5.5 was warmer than present day are found indirectly through estimates of accumulation rates as derived from chemical data (Wolff et al., 2010) or from unpublished measurements of ^{10}Be conducted on the Vostok ice core (Raisbeck, pers. comm.). Assuming a constant flux of ^{10}Be, these data suggest an ~20% increase in accumulation rate at MIS 5.5 compared to the Holocene. This rough estimate neglects other factors than can affect the deposition of ^{10}Be at Vostok, such as the spatial origin of the deep ice (upstream of Vostok), or changes in production for instance linked with the Blake geomagnetic event. EDC ^{10}Be and specific analyses of chemical species affected by accumulation-dependent post-depositional effects (such as nitrate (NO_3^-) and chloride (Cl^-)) may be used in the future to characterise EDC MIS 5.5 accumulation changes. The MIS 5.5 warming above present day is not restricted to Antarctica but is also found in ice core aerosol proxies linked with sea ice extent (Fischer et al., 2007) and observed in a variety of sea surface temperature reconstructions (reaching 1–4 °C above present day) at low latitudes (Medina-Elizalde and Lea, 2005; Lawrence et al., 2006), south of New Zealand (Barrows et al., 2007) and in various locations of the Southern Ocean (Bianchi and Gersonde, 2002; Govin et al., 2009).

Several coupled climate model simulations have now been run with the orbital forcing of MIS 5.5, and this will be a new target of the Paleoclimate Modelling Intercomparison Project (http://pmip2.lsce.ipsl.fr/share/overview/PMIP_flier_view.pdf). The differences between the present interglacial and MIS 5.5 are linked to a stronger eccentricity, and different phases between obliquity and precession configurations. Seasonal insolation anomalies are particularly large in the northern hemisphere for MIS 5.5 between 130 and 125 ka BP, reaching up to 70 W m^{-2} in summer (Berger and Loutre, 1991; Masson-Delmotte et al., 2006b) (Fig. 4).

Fig. 8 displays the results of four climate models, IPSL CM4 (Braconnot et al., 2008) and ECHAM5-MPIOM (both run under 126 ky BP orbital forcing), NCAR CCSM (Otto-Bliesner et al., 2006) (run under 130 ky BP orbital forcing) and an accelerated simulation of MPI-UW ESM run from 130 to 115 ky BP (Gröger et al., 2007) and for which we have averaged the outputs between 128 and 126 ky BP after verifying that the results are robust over this time period. Pre-industrial climate simulations have been used as references for three of the models. The CCSM control simulation is run in equilibrium with 1990 greenhouse gas concentrations. There can be significant differences due to different control simulations: for CCSM3, the "1990 greenhouse gas level" simulation is 1.2 °C warmer in Antarctica than a pre-industrial simulation.

For Greenland, all models clearly show a strong response to the enhanced northern latitude summer insolation, with a maximum warming in summer reaching ~3 to ~6 °C. Three of the models show a cooling in winter (~ −1 °C) and one model simulates a year-round warming, including a 2 °C persistent warming in winter. The annual mean temperature change simulated by the climate models varies between ~0.5 °C and 3 °C (see legend of Fig. 8). As all models simulate more snowfall during the warmer summer, their precipitation weighted annual temperature is systematically higher (~1 to ~3.6 °C). Two models clearly underestimate both the annual and precipitation weighted temperature change when compared to ice core data. The two other models simulate magnitudes of summer or precipitation weighted temperature changes (3–5 °C) which are compatible with the Greenland ice core based temperature estimates (~5 °C). For Greenland, it is remarkable that climate feedbacks associated with changes in high latitude intermediate and surface ocean temperature and sea ice cover (and vegetation in MPI-UW ESM) do transmit the summer insolation forcing all year round. Earlier studies had highlighted the importance of sea ice, snow, vegetation and water vapour feedbacks in the response to seasonal changes in insolation (Kubatzki et al., 2000; Khodri et al., 2005; Braconnot et al., 2007).

For Antarctica, the model-data comparison remains very frustrating. All four models do simulate a shift of the seasonal cycle (warmer temperatures by up to 4 °C in Antarctic spring but colder temperatures by up to 2 °C in Antarctic autumn). This is a linear response to the austral insolation forcing, where precession effects are maximum in Antarctic spring and autumn for MIS 5.5. In earlier studies, some authors have chosen to select the Antarctic spring temperature simulated by their models in order to highlight the importance of austral spring insolation on polar climate (Stott et al., 2007) via sea ice albedo feedbacks (Timmermann et al., 2009). However, the precipitation weighted information does not bring model outputs closer to ice core data. When considering annual mean averages, the three climate models show very little average annual temperature changes (between −0.7 °C and +0.4 °C, with a strong inter-annual variability). As a result of a parallel shift of the seasonal cycle of precipitation, the precipitation weighted annual temperature average (which is expected to be the model output most comparable with ice core data) ranges between −1.4 °C and +0.1 °C.

Four climate models therefore all display a robust pattern of changes for MIS 5.5 in central Antarctica, with a linear response to the shift of the austral seasonal cycle of insolation and no significant change in annual mean temperature. This is in sharp contrast with the ice core data. A similar mismatch is also observed for the early Holocene (optimum based on Antarctic stable isotopes versus no change based on climate models).

What can explain the model-data mismatch for Antarctica? Three different mechanisms involving missing cryospheric feedbacks can be invoked: (i) impact of Antarctic ice sheet topography; (ii) inadequate climate model response to changes in obliquity; (iii) missing feedbacks.

First, it was suggested that the mismatch may be caused by changes in atmospheric circulation around Antarctica in relationship with changes in Antarctic ice sheet topography at MIS 5.5 (Otto-Bliesner et al., 2006). The 4–6 m sea level high stand is thought to result both from South Greenland and West Antarctica (IPCC, 2007). If the peak isotopic anomaly of central Antarctic ice cores (respectively the MIS 5.5 plateau) had to be explained by local elevation, one would require a 500 m (respectively 200 m) lower elevation, which seems inconsistent with the observations in terms of accumulation, ice sheet dynamics and sea level fluctuations, and with the time scale of ice sheet reaction. Local elevation changes are poor candidates to explain the model-data mismatch. Another option is that a reduced West Antarctic Ice Sheet (e.g. Pollard and DeConto, 2009) could have an impact on Antarctic atmospheric

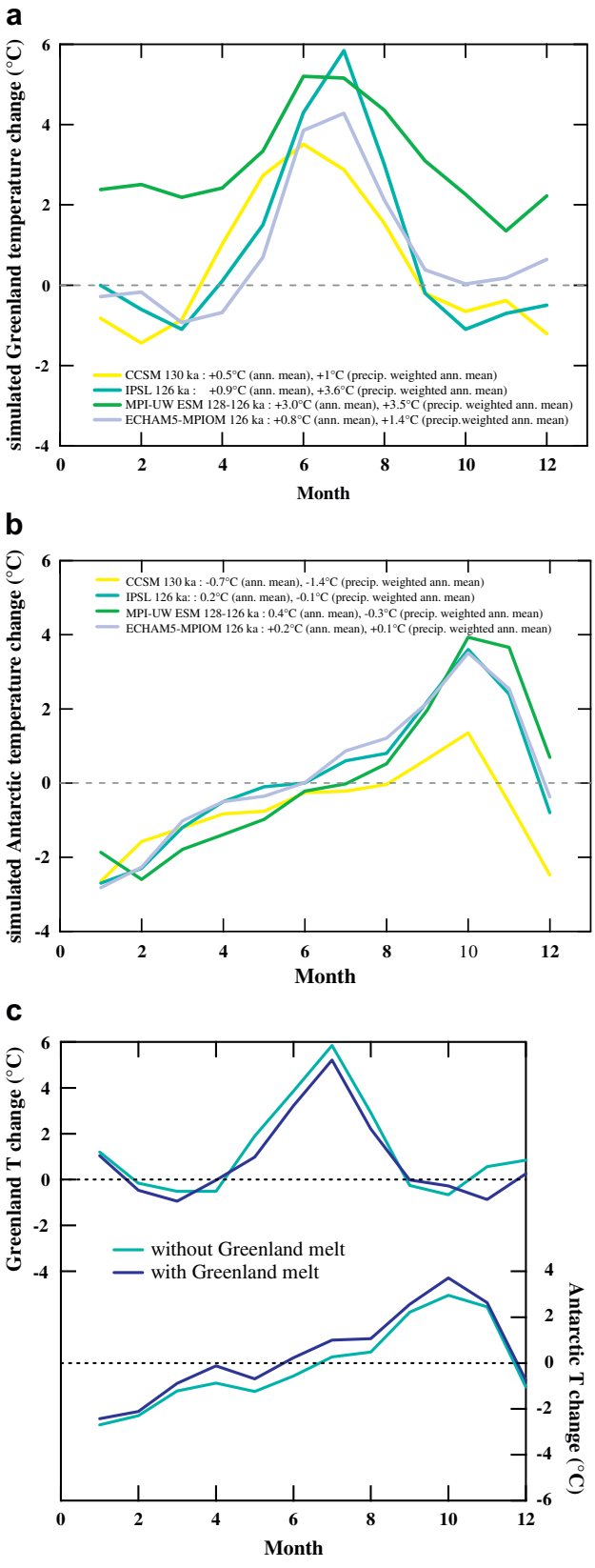

dynamics and induce a dynamical warming in central inland Antarctica. This hypothesis deserves to be further quantitatively explored with general circulation models in response to different ice sheet topographies.

Second, we have observed a strong imprint of obliquity in the EDC data. Obliquity is the only component of the orbital forcing which leaves a symmetric imprint at high latitudes north and south. The model-data mismatch may arise from a lack of simulated response to obliquity, involving a synchronous warming of the equatorial Pacific and of Antarctica. The MIS 5.5 warming above present day is indeed not restricted to Antarctica but is also observed in a variety of sea surface temperature reconstructions (reaching 1–4 °C above present day) at low latitudes (Medina-Elizalde and Lea, 2005; Lawrence et al., 2006), south of New Zealand (Barrows et al., 2007) and in various locations of the Southern Ocean (Bianchi and Gersonde, 2002; Govin et al., 2009). Ice core deuterium excess data highlight the importance of obliquity in driving changes in Antarctic moisture origin (Vimeux et al., 2001). The simulations analysed here (Fig. 7) and sensitivity studies conducted under pre-industrial boundary conditions with the coupled IPSL climate model (not shown) display a negligible impact of obliquity on the simulated annual mean Antarctic temperature. The lack of response to the obliquity forcing may result from model biases, such as a lack of austral sea ice in control simulations and therefore a lack of positive feedbacks linked with sea ice retreat.

Finally, the model-data mismatch may result from processes not included in the set up of the modelling experiments. Recently, it was suggested that the early MIS 5.5 Antarctic peak warmth may result from a north south bipolar seesaw process linked with the dramatic inflow of glacial meltwater from the northern hemisphere ice sheets possibly including Greenland (Kelly et al., 2006), a suggestion based on the phase lag between methane and Antarctic temperature change, recently reinforced by the discovery of a very sharp change in EDC deuterium excess during MIS 5.5. We therefore suggest that climate models fail to capture MIS 5.5 Antarctic warming because they do not include the feedbacks associated with ice sheet melting and global ocean circulation changes. This hypothesis could be tested by prescribing freshwater forcing for MIS 5.5, by calculating Greenland meltwater inflow, or by fully coupling climate and ice sheet models. A first sensitivity experiment has been conducted with the IPSL model (Swingedouw et al., in press) including the crude representation of Greenland land ice melting previously used for future climate projections (Swingedouw et al., 2006). In this model version, the ice melting depends on the climate conditions over the ice sheet and is routed to the ocean, thereby affecting the salinity and density of the surface ocean. Swingedouw et al. (in press) have also shown that the impact of freshwater on the AMOC strength depends on the mean climate state. The orbital configuration at 126 ky BP induces a cumulative melting over 250 years leading to an additional freshwater input of about 13.5×10^{14} m^3 into the North Atlantic. This corresponds to a sea level rise of 1.6 mm yr^{-1}, consistent with

Fig. 8. Comparison of three different climate model simulations for MIS5e regarding changes in the mean seasonal cycle for Greenland (Fig. 8a) and Antarctica (Fig. 8b). Different boundary conditions were used depending on the orbital context. NCAR CCSM (Otto-Bliesner et al., 2006) is run under 130 ka BP orbital forcing. IPSL CM4 is run under 126 ka BP orbital forcing (Braconnot et al., 2007; Braconnot et al., 2008), and it is the same for ECHAM5-MPIOM. MPI-UW is run accelerated from 130 to 115 ka BP in response to changes in orbital forcing (Gröger et al., 2007); its outputs have been extracted for the period from 128 to 126 ka BP. For each model, changes in annual mean temperature and in annual mean – monthly precipitation weighted temperature are displayed in the legend. Fig. 8c displays the IPSL model results (126 kyr minus pre-industrial) in the standard PMIP2 simulation (light blue, as in Fig. 8a and b), and in a sensitivity test including a parameterization of Greenland ice sheet melt (Swingedouw et al., in revision) (dark blue).

the 1.1 mm yr^{-1} estimate from a longer simulation (Otto-Bliesner et al., 2006). Since the parameterization does not account for all the surface processes over the ice sheet, our simulated melting rate should be seen as an upper bound. This freshwater flux reduces AMOC (Atlantic Meridional Overturning Circulation) by about 6 Sv. This ocean circulation change damps Greenland warming by ~0.5 °C but generates a 0.5 °C year-round Antarctic warming (Fig. 8c). The temperature change is robust with respect to precipitation weighting (to mimic deposition in ice cores).

Part of the Antarctic temperature variations which cannot be explained by changes in global greenhouse gas radiative forcings may therefore involve large-scale heat and moisture transport processes, both at the scale of obliquity and at the scale of interglacial optima. This hypothesis has profound implications on the interpretation of the shape of EDC temperature variations along interglacials, with peak warmth potentially associated with maximum northern hemisphere ice sheet melting.

6. Conclusions and perspectives

The EDC ice core offers a wealth of information on past climate glacial–interglacial dynamics. We have discussed the uncertainties linked with the intensity of glacial and interglacial periods as derived from water stable isotope records, and shown limited effects of changes in local elevation. A deeper understanding of the uncertainties linked with changes in moisture origin will soon be provided by the full record of EDC deuterium excess data.

A solid knowledge of past Antarctic temperature changes is critical for the comparison with climate model results. Indeed, Antarctica is one of the areas where these climate models simulate a strong link between past or future local changes and past or future global temperature changes, suggesting that it has relevance for global climate sensitivity investigations. While these models suggest a 2 to 1 glacial–interglacial relationship between EDC and global temperature change, one has to keep in mind that the PMIP simulations are conducted with a prescribed LGM Antarctic ice sheet elevation which is not supported by glaciological models and which accounts for almost half of the simulated glacial–interglacial temperature change. Simulations of warmer Antarctic climates are needed to explore the uncertainties associated with isotope-based reconstructions for interglacials.

The comparison between EDC temperature estimates and other proxy records available from the same ice core is useful to identify robust features regarding the relative intensity of glacial and interglacial extrema. Without doubts, MIS 5.5 and 11 appear as the warmest interglacial periods, while MIS 14 is the coolest interglacial period. MIS 2, 12 and 16 appear as the strongest glacial maxima, while MIS 13 and 17 have a weak intensity. This comparison also reveals different sensitivities of the various proxy records regarding the characterisation of these different intensities. For instance, EDC temperature appears to saturate and show little dispersion from a glacial maximum to the other, while it captures large differences from one interglacial period to the next.

Different methods have been deployed to assess the relationships between EDC temperature, global temperature, and global radiative forcings. When considering the radiative forcing only due to ice sheet albedo and greenhouse gas concentrations, a simple calculation using a constant fast feedback climate sensitivity of 0.75 °C per W m^{-2} proves efficient to capture most of the glacial–interglacial global temperature changes. The data suggest that the climate sensitivity was higher during the most recent glacial–interglacial cycles (0–450 ka) than during the earlier ones (450–800 ka). This very simple approach confirms that most of the glacial–interglacial variations purely arise from climate feedbacks. It shows that the "lukewarm" early interglacials displayed by the EDC ice core can be quantitatively explained in response to a larger ice sheet albedo and lower greenhouse gas concentrations compared to the Holocene. Earth system models including cryosphere and carbon cycle feedbacks are needed to further understand why such different "levels of interglacials" have occurred.

In order to go beyond this first order approach, we have analysed the part of the EDC temperature variations which cannot be accounted for by changes in greenhouse gas radiative forcing. These two parameters exhibit a parabolic relationship which shows that the Antarctic response to the change in greenhouse gas radiative forcing is not linear and depends on the background climate state; feedbacks associated with water vapour and ice clouds are indeed expected to be variable between warm and cold climate states. The residual between EDC temperature and this residual fit displays a strong obliquity component, highlighting slow feedbacks linking Antarctic temperature and obliquity (with a lag of 5 ky). The available simulations conducted with climate models do not show a significant impact of obliquity on the simulated Antarctic temperature, which exhibits a seasonal shift driven by the local effect of precession. The long lag between obliquity and EDC temperature (5 ky) remains to be understood and probably requires the explicit coupling between ice sheet and climate models (Bintanja and Van de Wal, 2008). A long-term trend is identified prior to 400 ky BP. This trend suggests that long-term processes do alter the carbon cycle and the Antarctic temperature–radiative forcing relationships.

None of the radiative forcing approaches can explain the trends and intensities of EDC temperature along interglacial periods. This suggests that other factors such as changes in local topography or changes in meridional heat transport may be at play. For exploring this, we have focused on MIS 5.5 which is exceptionally warm in the EDC temperature record. Four comprehensive climate model simulations are available for this time period. They all show a linear response to the shifted MIS 5.5 seasonal cycle of local insolation, without significant annual mean change. The simulations differ significantly between Antarctica where there is no identified feedback transferring the seasonal orbital forcing to an annual mean climate response, and Greenland, where local feedbacks do amplify the summer response and propagate the impact of the summer insolation forcing all year round. We suggest that the MIS 5.5 optimum in Antarctica may result from an Antarctic heat piracy (a north/south seesaw behaviour but during the beginning of the interglacial period), possibly in response to the final deglaciation of the northern hemisphere ice sheets and to the associated freshwater flux. This hypothesis is supported by a sensitivity test conducted with the IPSL model in response to a parameterization of Greenland meltwater flux, showing a slight (0.5 °C) Antarctic warming.

Acknowledgments

We thank J.R. Petit, G. Raisbeck and M. Werner, A. Timmermann and two anonymous reviewers for constructive comments on the manuscript. This work is a contribution to the European Project for Ice Coring in Antarctica (EPICA), a joint European Science Foundation/European Commission scientific programme, funded by the EU (EPICA-MIS) and by national contributions from Belgium, Denmark, France, Germany, Italy, the Netherlands, Norway, Sweden, Switzerland and the United Kingdom. The main logistic support was provided by IPEV and PNRA (at Dome C) and AWI (at Dronning Maud Land). LSCE ice core work has been supported by ANR (Agence Nationale de la Recherche) PICC and NEEM-France projects. We acknowledge the modelling groups for providing their data for analysis, the CMIP (Climate Model Intercomparison

Project) and PMIP (Paleoclimate Modelling Intercomparison Project) for collecting and archiving the model data. This is EPICA publication 233 and LSCE publication 4017.

References

Ahn, J., Brook, E.J., 2008. Atmospheric CO_2 and climate on millennial time scales during the Last Glacial Maximum. Science 322, 83–85.

Barrows, T.T., Juggins, S., De Deckker, P., Calvo, E., Pelejero, C., 2007. Long-term sea surface temperature and climate change in the Australian–New Zealand region. Paleoceanography 22, PA2215.

Berger, A., Loutre, M.F., 1991. Insolation values for the climate of the last 10 million years. Quaternary Science Reviews 10, 297–317.

Bianchi, C., Gersonde, R., 2002. The Southern Ocean surface between Marine Isotope Stages 6 and 5d: shape and timing of climatic changes. Palaeogeography, Palaeoclimatology, Palaeoecology 187, 151–177.

Bintanja, R., Van de Wal, R., 2008. North American ice-sheet dynamics and the onset of 100,000-year glacial cycles. Nature 454, 869–872.

Bintanja, R., van de Wal, R., Oerlemans, J., 2005. Modelled atmospheric temperatures and global sea levels over the past million years. Nature 437, 125–128.

Braconnot, P., Otto-Bliesner, B., Harrison, S., et al., 2007. Results of PMIP2 coupled simulations of the Mid-Holocene and Last Glacial Maximum. Part 2: feedbacks with emphasis on the location of the ITCZ and mid- and high latitude heat budget. Climate of the Past 3, 279–296.

Braconnot, P., Marzin, C., Grégoire, L., Mosquet, E., Marti, O., 2008. Monsoon response to changes in Earth's orbital parameters: comparisons between simulations of the Eemian and of the Holocene. Climate of the Past 4, 281–294.

Caillon, N., Severinghaus, J.P., Jouzel, J., Barnola, J.M., Kang, J., Lipenkov, V.Y., 2003. Timing of atmospheric CO_2 and Antarctic temperature changes across termination III. Science 299, 1728–1731.

Cheddadi, R., Beaulieu, J.L., Jouzel, J., Andrieu-Ponel, V., Laurent, J.M., Reille, M., Raynaud, D., Bar-Hen, A., 2005. Similarity of vegetation dynamics during interglacial periods. Proceedings of the National Academy of Sciences of the United States of America 102, 13030–13043.

CLIMAP, 1981. Seasonal reconstructions of the Earth's surface at the Last Glacial Maximum. In: GSA Map and Chart Series, MC-36. Geological Society of America, Boulder, CO.

Connolley, W.M., 1996. The Antarctic temperature inversion. International Journal of Climatology 16, 1333–1342.

Crucifix, M., 2006. Does the Last Glacial Maximum constrain climate sensitivity? Geophysical Research Letters 33. doi:10.1029/2006GL027137.

Dreyfus, G., Jouzel, J., Bender, M., Landais, A., Masson-Delmotte, V., Leuenberger, M., 2010. Firn processes and δ15N: potential for a gas-phase climate proxy. Quarternary Science Reviews 29, 28–42.

Dreyfus, G., Parrenin, F., Lemieux-Dudon, B., Durand, G., Masson-Delmotte, V., Jouzel, J., Barnola, J.M., Panno, L., Spahni, R., Tisserand, A., Siegenthaler, U., Leuenberger, M., 2007. Anomalous flow below 2700 m in the EPICA Dome C ice core detected using $\delta^{18}O$ of atmospheric oxygen measurements. Climate of the Past 3, 341–353.

Ekaykin, A.A., 2003. Meteorological Regime of Central Antarctic and its Role in the Isotopic Composition of Snow Thickness. Université Joseph Fourier, Grenoble.

Ekaykin, A.A., Lipenkov, V.Y., Kuzmina, I., Petit, J.R., Masson-Delmotte, V., Johnsen, S.J., 2004. The changes in isotope composition and accumulation of snow at Vostok station, East Antarctica, over the past 200 years. Annals of Glaciology 39, 569–575.

EPICA-Community-Members, 2004. Eight glacial cycles from an Antarctic ice core. Nature 429, 623–628.

EPICA-Community-Members, 2006. One-to-one coupling of glacial climate variability in Greenland and Antarctica. Nature 444, 195–198.

Fischer, H., Fundel, F., Ruth, U., Twarloh, B., Wegner, A., Udisti, R., Becagli, S., Castellano, E., Morganti, A., Severi, M., Wolff, E., Littot, G., Röthlisberger, R., Mulvaney, R., Hutterli, M., Kaufmann, P., Federer, U., Lambert, F., Bigler, M., Hansson, M., Jonsell, U., De Angelis, M., Boutron, C., Siggaard-Andersen, M.-L., Steffensen, J.P., Barbante, C., Gaspari, V., Gabrielli, P., Wagenbach, D., 2007. Reconstruction of millenial changes in dust emission, transport and regional sea-ice coverage using the deep EPICA ice cores from the Atlantic and Indian Ocean sector of Antarctica. Earth and Planetary Science Letters 260, 340–354.

Fischer, H., Wahlen, M., Smith, J., Mastroiani, D., Deck, B., 1999. Ice core records of atmospheric CO_2 around the last three glacial terminations. Science 283, 1712–1714.

Gallée, H., Gorodetskaya, I., 2008. Validation of a limited area model over Dome C, Antarctic Plateau, during winter. Climate Dynamics. doi:10.1007/s00382-008-0499-y.

Genthon, C., Barnola, J.M., Raynaud, D., Lorius, C., Jouzel, J., Barkov, N.I., Korotkevich, Y.S., Kotlyakov, V.M., 1987. Vostok ice core: climatic response to CO_2 and orbital forcing changes over the last climatic cycle. Nature 329, 414–418.

Gersonde, R., Crosta, X., Abelmann, A., Armand, L., 2005. Sea-surface temperature and sea ice distribution of the Southern Ocean at the EPILOG Last Glacial Maximum—a circum-Antarctic view based on siliceous microfossil records. Quaternary Science Reviews 24, 869–896.

Govin, A., Michel, E., Labeyrie, L., Waelbroeck, C., Dewilde, F., Jansen, E., 2009. Evidence for northward expansion of Antarctic Bottom water mass in the Southern Ocean during the last glacial inception. Paleoceanography 24. doi:10.1029/2008PA001603.

Gröger, M., Maier-Reimer, E., Mikolajewicz, U., Schurgers, G., Vizcaino, M., Wingurth, A., 2007. Changes in the hydrological cycle, ocean circulation and carbon/nutrient cycling during the Last Interglacial and glacial transitions. Paleoceanography 22, PA4205. doi:10.1029/2006PA001375.

Hansen, J., Sato, M., Kharecha, P., Beerling, D., Berner, R., Masson-Delmotte, V., Pagani, M., Raymo, M.E., Royer, D.L., Zachos, J.C., 2008. Target atmospheric CO_2: where should humanity aim? Open Atmospheric Sciences 2, 217–231.

Hargreaves, J.C., Abe-Ouchi, A., Annan, J.D., 2007. Linking glacial and future climates through an ensemble of GCM simulations. Climate of the Past 3, 77–87.

Hourdin, F., Musat, I., Bony, S., Braconnot, P., Codron, F., Dufresne, J.L., Fairhead, L., Filiberti, M.A., Friedlingstein, P., Grandpeix, J.Y., Krinner, G., Levan, P., Li, Z.X., Lott, F., 2006. The LMDZ4 general circulation model: climate performance and sensitivity to parameterizations. Climate Dynamics 27, 787–813.

Huybers, P., Denton, G.H., 2008. Antarctic temperature at orbital timescales controlled by local summer duration. Nature Geosciences 1, 787–792.

IPCC, 2007. Climate Change 2007 – The Physical Science Basis. Cambridge University Press, Cambridge.

Joos, F., 2005. Radiative forcing and the ice core greenhouse gas record. PAGES News 13, 11–13.

Joussaume, S., Taylor, K.E., 1995. Status of the Paleoclimate Modeling Intercomparison Project (PMIP). In: Proceedings of the first international AMIP scientific conference, WCRP 92, pp. 425–430.

Jouzel, J., Masson-Delmotte, V., Cattani, O., Dreyfus, G., Falourd, S., Hoffmann, G., Minster, B., Nouet, J., Barnola, J.M., Chappellaz, J., Fischer, H., Gallet, J.C., Johnsen, S., Leuenberger, M., Loulergue, L., Luethi, D., Oerter, H., Parrenin, F., Raisbeck, G., Raynaud, D., Schilt, A., Schwander, J., Selmo, E., Souchez, R., Spahni, R., Stauffer, B., Steffensen, J.P., Stenni, B., Stocker, T.F., Tison, J.L., Werner, M., Wolff, E., 2007. Orbital and millenial Antarctic climate variability over the past 800,000 years. Science 317, 793–796.

Jouzel, J., Vimeux, F., Caillon, N., Delaygue, G., Hoffmann, G., Masson-Delmotte, V., Parrenin, F., 2003. Magnitude of the isotope–temperature scaling for interpretation of central Antarctic ice cores. Journal of Geophysical Research 108, 1029–1046.

Kawamura, K., Parrenin, F., Lisiecki, L., Uemura, R., Vimeux, F., Severinghaus, J.P., Hutterli, M.A., Nakazawa, T., Aoki, S., Jouzel, J., Raymo, M.E., Matsumoto, K., Nakata, H., Motoyama, H., Fujita, S., Goto-Azuma, K., Fujii, Y., Watanabe, O., 2007. Northern Hemisphere forcing of climatic cycles in Antarctica over the past 360,000 years. Nature 448, 912–915.

Kelly, M.J., Edwards, R.L., Cheng, H., Yuan, D.X., Cai, Y., Zhang, M., An, Z., 2006. High resolution characterization of the Asian Monsoon between 146,000 and 99,000 years BP from Dongge Cave, China and global correlation of events surrounding Termination II. Palaeogeography, Palaeoclimatology, Palaeoecology 236, 20–38.

Khodri, M., Cane, M., Kukla, G., Gavin, J., Braconnot, P., 2005. The impact of precession changes on the Arctic climate during the Last Interglacial. Earth and Planetary Science Letters 236, 285–304.

Köhler, P., Bintanja, R., Fischer, H., Joos, F., Knutti, R., Lohmann, G., Masson-Delmotte, V., 2010. What caused Earth's temperature variations during the last 800,000 years? Data-based evidence on radiative forcing and constraints on climate sensitivity. Quaternary Science Reviews 29, 129–145.

Krinner, G., Genthon, C., Jouzel, J., 1997. GCM analysis of local influences on ice core δ signals. Geophysical Research Letters 24, 2825–2828.

Krinner, G., Werner, M., 2003. Impact of precipitation seasonality changes on isotopic signals in polar ice cores. Earth and Planetery Science Letters 216, 525–538.

Kubatzki, C., Montoya, M., Rahmstorf, S., Ganopolsk, i.A., Claussen, H., 2000. Comparison of the Last Interglacial climate simulated by a coupled global model of intermediate complexity and an AOGCM. Climate Dynamics 16, 799–814.

Lambert, F., Delmonte, B., Petit, J.R., Bigler, M., Kaufman, P.R., Hutterli, M., Stocker, T.F., Ruth, U., Steffensen, J.P., Maggi, V., 2008. Dust–climate couplings over the past 800,000 years from the EPICA Dome C ice core. Nature 452, 616–619.

Landais, A., Chappellaz, J., Delmotte, M., Jouzel, J., Blunier, T., Bourg, C., Caillon, N., Cherrier, S., Malaizé, B., Masson-Delmotte, V., Raynaud, D., Schwander, J., Steffensen, J.P., 2003. A tentative reconstruction of the Greenland Eemian and glacial inception based on gas measurements in the GRIP ice core. Journal of Geophysical Research 108, 1–8. D06103.

Landais, A., Masson-Delmotte, V., Jouzel, J., Raynaud, D., Johnsen, S., Huber, C., Leuenberger, M., Schwander, J., Minster, B., 2005. The glacial inception recorded in the NorthGRIP Greenland ice core: information from air isotopic measurements. Climate Dynamics 26. doi:10.1007/s00382-005-0063-y.

Laskar, J., Joutel, F., Boudin, F., 1993. Orbital, precessional, and insolation quantities for the Earth from −20Myr to +10Myr. Astronomy and Astrophysics 270, 522–533.

Lawrence, K.T., Liu, Z.H., Herbert, T.D., 2006. Evolution of the eastern tropical Pacific through Plio–Pleistocene glaciation. Science 312, 79–83.

Lea, D.W., 2004. The 100 000-Yr cycle in tropical SST, greenhouse forcing, and climate sensitivity. Journal of Climate 17, 2170–2179.

Li, Z.X., Treut, H.L., 1992. Cloud radiation feedbacks in a general circulation model and their dependence on cloud modelling assumptions. Climate Dynamics 7, 133–139.

Lisiecki, L.E., Raymo, M.E., 2005. A Pliocene–Pleistocene stack of 57 globally distributed benthic d18O records. Paleoceanography 20. doi:10.1029/2004PA001071.

Lorius, C., Jouzel, J., Raynaud, D., Hansen, J., Le Treut, H., 1990a. Greenhouse warming, climate sensitivity and ice core data. Nature 347, 139–145.
Lorius, C., Jouzel, J., Raynaud, D., Hansen, J., Le Treut, H., 1990b. The ice-core record: climate sensitivity and future greenhouse warming. Nature 347, 139–145.
Loulergue, L., Parrenin, F., Blunier, T., Barnola, J.-M., Spahni, R., Schilt, A., Raisbeck, G., Chappellaz, J., 2007. New constraints on the gas age–ice age difference along the EPICA ice cores, 0–50 kyr. Climate of the Past 3, 527–540.
Loulergue, L., Schilt, A., Spahni, R., Masson-Delmotte, V., Blunier, T., Lemieux, B., Barnola, J.M., Raynaud, D., Stocker, T., Chappelaz, J., 2008. Orbital and millennial-scale features of atmospheric CH_4 over the last 800 000 years. Nature 453, 383–386.
Lüthi, D., Floch, M.L., Bereiter, B., Blunier, T., Barnola, J.M., Siegenthaler, U., Raynaud, D., Jouzel, J., Fischer, H., Kawamura, K., Stocker, T.F., 2008. High resolution carbon dioxide concentration record 650,000–800,000 years before present. Nature 453, 379–382.
Masson-Delmotte, V., Dreyfus, G., Braconnot, P., Johnsen, S., Jouzel, J., Kageyama, M., Landais, A., Loutre, M.F., Nouet, J., Parrenin, F., Raynaud, D., Stenni, B., Tuenter, E., 2006b. Past temperature reconstructions from deep ice cores: relevance for future climate change. Climate of the Past 2, 145–165.
Masson-Delmotte, V., Hou, S., Ekaykin, A., Jouzel, J., Aristarain, A., Bernardo, R.T., Bromwhich, D., Cattani, O., Delmotte, M., Falourd, S., Frezzotti, M., Gallée, H., Genoni, L., Isaksson, E., Landais, A., Helsen, M., Hoffmann, G., Lopez, J., Morgan, V., Motoyama, H., Noone, D., Oerter, H., Petit, J.R., Royer, A., Uemura, R., Schmidt, G.A., Schlosser, E., Simões, J.C., Steig, E., Stenni, B., Stievenard, M., Broeke, M.v.d., Wal, R.v.d., Berg, W.-J.v.d., Vimeux, F., White, J.W.C., 2008. A review of Antarctic surface snow isotopic composition: observations, atmospheric circulation and isotopic modelling. Journal of Climate 21, 3359–3387.
Masson-Delmotte, V., Jouzel, J., Landais, A., Stievenard, M., Johnsen, S.J., White, J.W.C., Sveinbjornsdottir, A., Fuhrer, K., 2005. Deuterium excess reveals millennial and orbital scale fluctuations of Greenland moisture origin. Science 309, 118–121.
Masson-Delmotte, V., Kageyama, M., Braconnot, P., Charbit, S., Krinner, G., Ritz, C., Guilyardi, E., Jouzel, J., Abe-Ouchi, A., Crucifix, M., Gladstone, R.M., Hewitt, C.D., Kitoh, A., Legrande, A., Marti, O., Merkel, U., Motoi, T., Ohgaito, R., Otto-Bliesner, B., Peltier, R.W., Ross, I., Valdes, P., Vettoretti, G., Weber, S.L., Wolk, F., 2006a. Past and future polar amplification of climate change: climate model intercomparisons and ice-core constraints. Climate Dynamics. doi:10.1007/s00382-005-0081-9.
Medina-Elizalde, M., Lea, D.W., 2005. The Mid-Pleistocene transition in the tropical Pacific. Science 310, 1009–1012.
Monnin, E., Indermühle, A., Dällenbach, A., Flückiger, J., Stauffer, B., Stocker, T., Raynaud, D., Barnola, J.M., 2001. Atmospheric CO_2 concentrations over the last glacial termination from the Dome Concordia, Antarctica, ice core. Science 291, 112–114.
NorthGRIP-Community-Members, 2004. High resolution climate record of the northern hemisphere reaching into Last Interglacial period. Nature 431, 147–151.
Otto-Bliesner, B., 2009. A comparison of PMIP2 model simulations and the MARGO proxy reconstruction for tropical sea surface temperatures at the last glacial maximum. Climate Dynamics 32, 799–815.
Otto-Bliesner, B.L., Marshall, S.J., Overpeck, J.T., Miller, G.H., Hu, A., and members, C. l. i. p., 2006. Simulating Arctic climate warmth and icefield retreat in the Last Interglaciation. Science 311, 1751–1753.
Paillard, D., 1998. The timing of Pleistocene glaciations from a simple multiple-state climate model. Nature 391, 378–381.
Parrenin, F., Barnola, J.M., Beer, J., Blunier, T., Castellano, E., Chappellaz, J., Dreyfus, G., Fischer, H., Fujita, S., Jouzel, J., Kawamura, K., Lemieux-Dudon, B., Loulergue, L., Masson-Delmotte, V., Narcisi, B., Petit, J.R., Raisbeck, G., Raynaud, D., Ruth, U., Schwander, J., Severi, M., Spahni, R., Steffensen, J.P., Svensson, A.M., Udisti, R., Waelbroeck, C., Wolff, E., 2007a. The EDC3 chronology for the EPICA Dome C ice core. Climate of the Past 3, 485–497.
Parrenin, F., Dreyfus, G., Durand, G., Fujita, S., Gagliardini, O., Gillet, F., Jouzel, J., Kawamura, K., Lhomme, N., Masson-Delmotte, V., Ritz, C., Schwander, J., Shoji, H., Uemura, R., Yoshida, N., Watanabe, O., Wolff, E.W., 2007b. Ice flow modelling at Dome C and Dome Fuji, East Antarctica. Climate of the Past 3, 243–259.
Peltier, W.R., 2004. Global glacial isostasy and the surface of the ice-age Earth: the ICE-5G (VM2) model and GRACE. Annual Review of Earth and Planetary Sciences 32, 111–149.
Peltier, W.R., Delmonte, B., 2009. A model for large glacial–interglacial climate-induced changes in dust and sea salt concentrations in deep ice cores (central Antarctica): palaeoclimatic implications and prospects for refining ice core chronologies. Tellus 61B 32, 768–790.
Petit, J.R., Jouzel, J., Raynaud, D., Barkov, N.I., Barnola, J.-M., Basile, I., Bender, M., Chappellaz, J., Davis, J., Delaygue, G., Delmotte, M., Kotlyakov, V.M., Legrand, M., Lipenkov, V., Lorius, C., Pépin, L., Ritz, C., Saltzman, E., Stiévenard, M., 1999. Climate and atmospheric history of the past 420000 years from the Vostok ice core, Antarctica. Nature 399, 429–436.
Pol, K., Masson-Delmotte, V., Jouzel, J., Li, L., Kageyama, M., Braconnot, P., Gallée, H., 2008. EPICA Dome C radiative forcing calculationsEGU General Assembly. Geophysical Research Abstracts, Vienna, Austria, pp. EGU2008-A-07704.
Pollard, D., DeConto, R.M., 2009. Modelling West Antarctic ice sheet growth and collapse through the past five million years. Nature 458, 329–332.
Röthlisberger, R., Mudelsee, M., Bigler, M., Angelis, M., d., Fischer, H., Hansson, M., Lambert, F., Masson-Delmotte, V., Sime, L., Udisti, R., Wolff, E.W., 2008. The southern hemisphere at glacial terminations: insights from the Dome C ice core. Climate of the Past 4, 345–356.
Schmittner, A., Galbraith, E.D., 2008. Glacial greenhouse-gas fluctuations controlled by ocean circulation changes. Nature 456, 373–376.
Schneider von Deimling, T., Held, H., Ganopolski, A., Rahmstorf, S., 2006. Climate sensitivity estimated from ensemble simulations of glacial climate. Climate Dynamics. doi:10.1007/s00382-006-0126-8.
Siegenthaler, U., Stocker, T.F., Monnin, E., Lüthi, D., Schwander, J., Stauffer, B., Raynaud, D., Barnola, J.-M., Fischer, H., Masson-Delmotte, V., Jouzel, J., 2005. Stable carbon cycle–climate relationship during the last Pleistocene. Science 310, 1313–1317.
Sosdian, S., Rosenthal, Y., 2009. Deep-sea temperature and ice volume changes across the Pliocene–Pleistocene climate transitions. Science 325, 306–310.
Spahni, R., Chappellaz, J., Stocker, T.F., Loulergue, L., Hausammann, G., Kawamura, K., Flückiger, J., Schwander, J., Raynaud, D., Masson-Delmotte, V., Jouzel, J., 2005. Variations of atmospheric methane and nitrous oxide during the last 650,000 years from Antarctic ice cores. Science 310, 1317–1321.
Stenni, B., Masson-Delmotte, V., Selmo, E., Oerter, H., Meyer, H., Röthlisberger, R., Jouzel, J., Cattani, O., Falourd, S., Fischer, H., Hoffmann, G., Iacumin, P., Johnsen, S.J., Minster, B., Udisti, R., 2010. The deuterium excess records of EPICA Dome C and Dronning Maud Land ice cores (East Antarctica). Quaternary Science Reviews 29, 146–159.
Stenni, B., Masson, V., Johnsen, S.J., Jouzel, J., Longinelli, A., Monnin, E., Rothlisberger, R., Selmo, E., 2001. An oceanic cold reversal during the last deglaciation. Science 293, 2074–2077.
Stocker, T., Johnsen, S., 2003. A minimum thermodynamic model for the bipolar seesaw. Paleoceanography 18, 1087.
Stott, L., Timmermann, A., Thunell, R., 2007. Southern hemisphere and deep-sea warming led deglacial atmospheric CO_2 rise and tropical warming. Science 318, 435–438.
Sun, Y.B., Clemens, S.C., An, Z.S., Yu, Z.W., 2006. Astronomical time scale and palaeoclimatic implication of stacked 3.6-Myr monsoon records from the Chinese Loess Plateau. Quaternary Science Reviews 25, 33–48.
Swingedouw, D., Braconnot, P., Marti, O., 2006. Sensitivity of the Atlantic Meridional Overturning Circulation to the melting from northern glaciers in climate change experiments. Geophysical Research Letters 33. doi:10.1029/2006GL025765.
Swingedouw, D., Mignot, J., Braconnot, P., Mosquet, E., Kageyama, M., Alkama, R. Impact of freshwater release in the North Atlantic under different climate conditions in an OAGCM, in press, doi:10.1175/2009JCLI3028.1.
Timmermann, A., Timm, O., Stott, L., Menviel, L., 2009. The roles of CO_2 and orbital forcing in driving southern hemispheric temperature variations during the last 21,000 years. Journal of Climate 22, 1626–1640.
Tzedakis, P.C., Hooghiemstra, H., Palike, H., 2006. The last 1.35 million years at Tenaghi Philippon: revised chronostratigraphy and long-term vegetation trends. Quaternary Science Reviews 25, 23–24.
Vimeux, F., Cuffey, K., Jouzel, J., 2002. New insights into Southern Hemisphere temperature changes from Vostok ice cores using deuterium excess correction over the last 420,000 years. Earth and Planetary Science Letters 203, 829–843.
Vimeux, F., Masson, V., Delaygue, G., Jouzel, J., Petit, J.-R., Stievenard, M., 2001. A 420,000 year deuterium excess record from East Antarctica: information on past changes in the origin of precipitation at Vostok. Journal of Geophysical Research 106, 31863–31873.
Vimeux, F., Masson, V., Jouzel, J., Stievenard, M., Petit, J.R., 1999. Glacial–interglacial changes in ocean surface conditions in the Southern Hemisphere. Nature 398, 410–413.
Wang, Y., Cheng, H., Edwards, R.L., King, X., Shao, X., Chen, S., Wu, J., Jiang, X., Wang, X., An, Z., 2008. Millennial and orbital-scale changes in the East Asian monsoon over the past 224,000 years. Nature 451, 1090–1093.
Watanabe, O., Jouzel, J., Johnsen, S., Parrenin, F., Shoji, H., Yoshida, N., 2003. Homogeneous climate variability across East Antarctica over the past three glacial cycles. Nature 422, 509–512.
Wolff, E.W., Barbante, C., Becagli, S., Bigler, M., Boutron, C.F., Castellano, E., de Angelis, M., Federer, U., Fischer, H., Fundel, F., Hansson, M., Hutterli, M., Jonsell, U., Karlin, T., Kaufmann, P., Lambert, F., Littot, G.C., Mulvaney, R., Röthlisberger, R., Ruth, U., Severi, M., Siggaard-Andersen, M.L., Sime, L.C., Steffensen, J.P., Stocker, T.F., Traversi, R., Twarloh, B., Udisti, R., Wagenbach, D., Wegner, A., 2010. Changes in environment over the last 800 000 years from chemical analysis of the EPICA Dome C ice core. Quaternary Science Reviews 29, 285–295.
Wolff, E.W., Fischer, H., Fundel, F., Ruth, U., Twarloh, B., Littot, G., Mulvaney, R., Röthlisberger, R., De Angelis, M., Boutron, C., Hansson, M., Jonsell, U., Hutterli, M., Lambert, F., Kaufmann, P., Stauffer, B., Stocker, T.F., Steffensen, J.P., Bigler, M., Siggaard-Andersen, M.-L., Udisti, R., Becagli, S., Castellano, E., Severi, M., Wagenbach, D., Barbante, C., Gabrielli, P., Gaspari, V., 2006. Southern Ocean sea-ice extent, productivity and iron flux over the past eight glacial cycles. Nature 440, 491–496.
Wolff, E.W., Fischer, H., Röthlisberger, R., 2009. Glacial terminations as southern warmings without northern control. Nature Geosciences 2, 206–209.
Zachos, J.C., Shackleton, N.J., Revenaugh, J.S., Pälike, H., Flowers, B.P., 2001. Climate response to orbital forcing across the Oligocene–Miocene boundary. Science 292, 274–277.